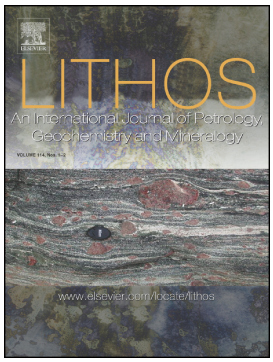


# Insights into the evolution of an alkaline magmatic system: An in situ trace element study of clinopyroxenes from the Ditrău Alkaline Massif, Romania

Anikó Batki, Elemér Pál-Molnár, M. Éva Jankovics, Andrew C. Kerr, Balázs Kiss, Gregor Markl, Adrián Heincz, Szabolcs Harangi

PII: S0024-4937(17)30414-0
DOI: doi:10.1016/j.lithos.2017.11.029
Reference: LITHOS 4490

To appear in:

Received date: 7 August 2017
Accepted date: 28 November 2017

Please cite this article as: Anikó Batki, Elemér Pál-Molnár, M. Éva Jankovics, Andrew C. Kerr, Balázs Kiss, Gregor Markl, Adrián Heincz, Szabolcs Harangi , Insights into the evolution of an alkaline magmatic system: An in situ trace element study of clinopyroxenes from the Ditrău Alkaline Massif, Romania. The address for the corresponding author was captured as affiliation for all authors. Please check if appropriate. Lithos(2017), doi:10.1016/j.lithos.2017.11.029

# Insights into the evolution of an alkaline magmatic system: an in situ trace element study of clinopyroxenes from the Ditrău Alkaline Massif, Romania

Anikó Batki[a,b,*,1], Elemér Pál-Molnár[a,b,1], M. Éva Jankovics[a,b], Andrew C. Kerr[c], Balázs Kiss[a,b], Gregor Markl[d], Adrián Heincz[b], Szabolcs Harangi[a]

[a] MTA-ELTE Volcanology Research Group, Pázmány Péter sétány 1/C, H-1117 Budapest, Hungary

[b] 'Vulcano' Petrology and Geochemistry Research Group, Department of Mineralogy, Geochemistry and Petrology, University of Szeged, Egyetem Street 2, H-6722 Szeged, Hungary

[c] School of Earth and Ocean Sciences, Cardiff University, Main Building, Cardiff CF10 3AT, United Kingdom

[d] Fachbereich Geowissenschaften, Universität Tübingen, Wilhelmstrasse 56, D-72074 Tübingen, Germany

*Corresponding author. Telephone: 003613722500 8359. Fax: 003613812108. E-mail: aniko.batki@gmail.com

[1]The first two authors have contributed equally to this work.



**Abstract**

Clinopyroxene is a major constituent in most igneous rock types (hornblendite, diorite, syenite, nepheline syenite, camptonite, tinguaite and ijolite) of the Ditrău Alkaline Massif, Eastern Carpathians, Romania. Phenocryst and antecryst populations have been distinguished based on mineral zoning patterns and geochemical characteristics. Major and trace element

compositions of clinopyroxenes reflect three dominant pyroxene types including primitive high-Cr Fe-diopside, intermediate Na-diopside-hedenbergite and evolved high-Zr aegirine-augite. Clinopyroxenes record two major magma sources as well as distinct magma evolution trends. The primitive diopside population is derived from an early camptonitic magma related to basanitic parental melts, whilst the intermediate diopside-hedenbergite crystals represent a Na-, Nb- and Zr-rich magma source recognised for the first time in the Ditrău magmatic system. This magma fractionated towards ijolitic and later phonolitic compositions. Field observations, petrography and clinopyroxene-melt equilibrium calculations reveal magma recharge and mingling, pyroxene recycling, fractional crystallisation and accumulation. Repeated recharge events of the two principal magmas resulted in multiple interactions between more primitive and more fractionated co-existing magma batches. Magma mingling occurred between mafic and felsic magmas by injection of ijolitic magma into fissures (dykes) containing phonolitic (tinguaite) magma. This study shows that antecryst recycling, also described for the first time in Ditrău, is a significant process during magma recharge and demonstrates that incorporated crystals can crucially affect the host magma composition and so whole-rock chemical data should be interpreted with great care.

**Keywords:** Clinopyroxene; Alkaline igneous complex; LA-ICP-MS; Zoning patterns; Antecryst recycling; Magma recharge

## 1. Introduction

Open- and closed-system magma chamber processes such as magma mixing, mingling, recharge, crystal mush remobilisation, crystallisation and assimilation significantly affect the evolution of different magmas in the lithosphere as well as their volcanic activity.

Investigation of exhumed magma reservoirs, i.e., plutonic systems, can significantly contribute to our understanding these magmatic processes (e.g., Frost and Mahood, 1987; Barbarin and Didier, 1992; Kerr et al., 1999; Baxter and Feely, 2002; Weidendorfer et al., 2014; Michel et al., 2016; Ma et al., 2017).

The textural, zoning and compositional characteristics of clinopyroxene in petrologically and geochemically diverse volcanic and plutonic rocks have been extensively studied over the past 40 years (e.g., Wass, 1979; Duda and Schmincke, 1985; Dobosi et al., 1991; Dobosi and Fodor, 1992; Neumann et al., 1999; Nakagawa et al., 2002; Streck et al., 2002; Marks et al., 2004; Shane et al., 2008; Stroncik et al., 2009; Winpenny and Maclennan, 2011; Jankovics et al., 2012, 2016; Ubide et al., 2014a, b; Gernon et al., 2016). These detailed mineral-scale studies have inferred the origin of different clinopyroxene populations, from open- and closed-system petrogenetic processes operating in subvolcanic magma storage systems to the evolution and ascent histories of different magmas (replenishment, magma mixing, mingling, xenocryst incorporation, fractional crystallisation and contamination). Based on these results, clinopyroxene is considered as a significant petrogenetic indicator that can be effectively used to unravel the evolution of magmatic systems.

The petrogenesis of the Ditrău Alkaline Massif has been in the focus of many studies in the last 150 years (e.g., Streckeisen, 1954, 1960; Codarcea et al., 1957; Streckeisen and Hunziker, 1974; Pál-Molnár and Árva-Sós, 1995; Dallmeyer et al., 1997; Kräutner and Bindea, 1998; Morogan et al., 2000; Pál-Molnár, 2000, 2010b; Fall et al., 2007; Batki et al. 2014; Pál-Molnár et al., 2015b). However, because of the wide range of lithologies and complex field relationships, contrasting models for the origin and magmatic evolution of the massif have been proposed. Since most of its rock types contain clinopyroxene, an integrated textural and

geochemical study of this mineral phase serves as a useful tool to unravel the succession and interactions of magmas as well as the deep-seated petrogenetic processes in the Ditrău plutonic system.

In this study, we present the textural varieties and a new major and trace element geochemical dataset of diverse clinopyroxene crystals from seven related rock types of the alkaline igneous suite of the Ditrău plutonic system. Textural and zoning characteristics are combined with chemical compositions to identify distinct phenocryst and antecryst populations. We use in-situ LA-ICP-MS data to carry out clinopyroxene-melt equilibrium calculations in order to reveal the dominant open- and closed-system magma chamber processes. Additionally, a new magma source has been discovered in the Ditrău magmatic system and further genetic relationships between the studied alkaline igneous rocks have been identified.

## 2. Geological setting

The Ditrău Alkaline Massif is a Mesozoic igneous complex located in the Eastern Carpathians, Romania (Fig. 1a). The massif outcrops immediately east of the Călimani–Gurghiu–Harghita Neogene–Quarternary volcanic chain (Fig. 1b) and is partly covered by andesitic pyroclastic deposits and lavas as well as by Pliocene–Pleistocene sediments (Codarcea et al., 1957; Pál-Molnár, 2010a). The igneous complex was formed during an extensional phase of the Alpine orogeny related to a rifted continental margin adjacent to Tethys. The intrusions are inferred to have been related to the opening events of the Meliata–Hallstatt ocean (Hoeck et al., 2009) where rifting is proposed to have commenced in the Pelsonian Substage (Middle Triassic) (Kozur, 1991).

The basement of the Eastern Carpathians is composed of Neoproterozoic to early Paleozoic peri-Gondwanan terranes that were variably affected by the Variscan orogeny, and so is similar to other basement terrains of Europe (Balintoni et al., 2014). The Ditrău Alkaline Massif lies within the Dacia Mega-Unit (Median Dacides; Săndulescu, 1984) of the Alpine–Carpathian–Dinaric region (Fig. 1a) and intrudes the Variscan metamorphic rocks that form the Alpine nappes in the Eastern Carpathians. The Alpine nappes from the bottom to the top are: the Bucovinian, the Subbucovinian and the Infrabucovinian Nappes. These nappes were thrust over each other during the Cretaceous (Austrian tectogenesis), and have an eastern vergence. Structurally, the Ditrău Alkaline Massif is the part of the lowermost Bucovinian Nappe, and is in direct contact with four of its Pre-Alpine Ordovician Gondwanan terranes (metamorphic units) (Bretila Terrane, Tulgheş Terrane, Negrişoara Terrane and Rebra Terrane; Balintoni et al., 2014).

The massif consists of a series of ultramafic and mafic cumulates grading to intermediate and felsic rocks from west to east (Pál-Molnár, 2000, Pál-Molnár et. al, 2015a, b). Hornblendite, gabbro and diorite are the dominant rock-types in the north- and central-west part of the igneous complex; monzonite, syenite, quartz syenite and granite extend from the north to the south-east, while nepheline syenite is concentrated in a large area of the central and eastern part of the massif (Fig. 1c). The whole massif is cut by numerous dykes including camptonites, tinguaites, alkali feldspar syenites and nepheline syenites.

The ultramafic rocks represent the oldest part of the Massif and were emplaced from 237 to 216 Ma, although their ages overlap that of the gabbros (234 Ma). The nepheline syenites and granites are younger, and have been dated at 232–216 Ma and 217–196 Ma, respectively. Ages have been obtained by K–Ar on hornblende, biotite, nepheline and feldspar separates

(Pál-Molnár and Árva-Sós, 1995), and a mid- to late-Triassic age of the early components was later confirmed by additional $^{40}Ar/^{39}Ar$ hornblende ages of 231 Ma and 227 Ma for gabbro and diorite, respectively (Dallmeyer et al., 1997). A U–Pb zircon age of 229.6 ± 1.7 Ma has been reported for the syenites (Pană et al., 2000).

A mantle origin for the mafic and ultramafic bodies was inferred by Kräutner and Bindea (1998) and by Morogan et al. (2000). Morogan et al. (2000) suggested that the massif was formed from primitive basanitic magmas that resulted from small-fraction asthenospheric melts, followed by progressive evolution to phonolitic residues. They attributed an important role to assimilation and fractionation, in conjunction with the mixing of felsic and basanitic melts. The hornblendites are interpreted as gravitational cumulates on a magma chamber floor (Pál-Molnár, 2000, 2010b; Pál-Molnár et al., 2015b) or as disrupted bodies of former side-wall cumulates (Morogan et al., 2000). Modelling suggests that camptonite dykes have been generated by 1–4% partial melting of an enriched, amphibole-bearing garnet lherzolite mantle source. These dykes represent the only primitive mafic melt known in the massif and therefore have been interpreted as the parental melts of the whole igneous complex (Batki et al., 2014).

## 3. Field relations and samples

Hornblendite cumulates are enclosed in gabbroic–dioritic rocks as lenticular or block-shaped bodies from a few centimetres to a hundred metres or more in size. The cumulates span a wide range of compositions but predominantly consist of olivine and/or clinopyroxene to essentially mono-mineralic hornblendite. A complete igneous rock series from hornblendite to gabbro, diorite, monzodiorite, monzonite, quartz monzonite, syenite, quartz syenite and

granite can be observed from the north-west to the north-east part of the massif (Pál-Molnár et al., 2015b) (Fig. 1c).

Syenites show mingling features with dioritic/gabbroic rocks (described as “Ditro essexite” by Streckeisen, 1960) (Fig. 2a). Nepheline syenites are the most abundant rocks of the massif and predominate in the eastern part and form large bodies and dykes.

Rare tinguaites, which are petrogenetically related to nepheline syenites (Streckeisen, 1954) form thin dykes crosscutting the granites, syenites and nepheline syenites. Additionally, small, discrete, rounded, ijolitic enclaves occur within some of the tinguaite dykes indicating mingling (mechanical interaction) of co-existing mafic and felsic magmas before solidification (e.g., Barbarin and Didier, 1991; Ubide et al., 2014c). The globular to lenticular dark grey ijolite enclaves with sharp margins vary in diameter from 1 to 9 centimetres (Fig. 2b).

Representative samples of rocks containing clinopyroxenes i.e., hornblendite cumulates, diorites, syenites, nepheline syenites, camptonites and tinguaite dykes including ijolite enclaves were collected from distinct parts of the Ditrău Alkaline Massif (Pietrăriei de Sus, Tarniţa de Jos, Teasc, Jolotca, Creanga Mare, Ditrău and Cetăţii Creeks) (Table 1, Fig. 1c). Hornblendite cumulate, nepheline syenite, camptonite, tinguaite and some of the ijolite samples have formed part of previous petrological and mineralogical studies (Fall et al., 2007; Batki et al., 2004; 2012a,b, 2014; Pál-Molnár, 2000; Pál-Molnár, 2010b, Batki and Pál-Molnár, 2011; Pál-Molnár et al., 2015b).

## 4. Petrography and whole rock geochemistry

*4.1. Hornblendite cumulate*

Hornblendite cumulates have been recently described by Pál-Molnár (2010b) and Pál-Molnár et al (2015). According to these studies, two cumulate types can be recognised: poikilitic olivine-bearing hornblendite cumulate, and pyroxene-rich hornblendite cumulate. The rocks are dark grey, coarse-grained, inequigranular and display orthocumulate and mesocumulate textures. Poikilitic olivine-bearing cumulates consist of up to 30 modal% olivine and 23% cumulus clinopyroxene enclosed by intercumulus amphibole oikocrysts. Pyroxene-rich cumulates comprising a nearly monomineralic assemblage of up to 90 vol.% amphibole accompanied by biotite (up to 10 vol.%), up to 16 vol.% clinopyroxene, ~5 vol.% plagioclase, ~5 vol.% apatite, ~3 vol.% titanite, and ~3 vol.% magnetite. Amphibole oikocrysts enclose small clinopyroxenes with sizes of around 450 µm (Fig. 2b in Pál-Molnár et al., 2015b). Brown-coloured, euhedral to subhedral, cumulus clinopyroxene is also present (Fig. 3a).

Olivine-bearing cumulates are the most primitive amongst the Ditrău mafic-ultramafic cumulate series with MgO contents of 16–17 wt.% and the highest Ni and Cr contrentrations (<390 ppm and <509 ppm, respectively). They are also the least enriched in rare earth element (REE) and have positive Pb, Hf and Ti and negative Zr and Y anomalies on primitive mantle-normalised diagrams. Pyroxene-rich cumulates have high alkali, $TiO_2$, $P_2O_5$ and $FeO^T$ contents and high Sr, Ba, Zr, Nb and Y concentrations (Table 2). Chondrite-normalised REE patterns have no Eu anomaly and are enriched in LREE, while primitive mantle-normalised patterns have negative P, Ti, U and K (Pál-Molnár et al., 2015b).

*4.2. Diorite*

The studied diorite is dark-to-light grey coloured, medium-grained with granular texture, and is composed of amphibole (44 vol.%), biotite (11 vol.%), plagioclase (35 vol.%), subordinate

clinopyroxene (4 vol.%), apatite, magnetite, and titanite. Anhedral clinopyroxene is surrounded by euhedral amphibole crystals (250–3000 µm sized) and subhedral biotite (up to 7.5 mm) (Fig. 3b).

The diorite is moderately evolved (mg# 0.4) and is compositionally similar to the Ditrău camptonites (Table 2). It plots in the basanitic field of the TAS diagram (not shown) with $SiO_2$ contents of 43 wt.% and total alkalis ($Na_2O$+$K_2O$) of 5.4 wt.%. The $TiO_2$ content is high (4 wt.%) and is a common feature of the Ditrău mafic rocks, along with high Nb, Zr, Sr, Ba and LREE enrichment.

*4.3. Syenite*

The greyish pink coloured syenite is inequigranular and medium- to fine-grained. It consists of amphibole (2 vol.%), biotite (1 vol.%), potassium feldspar (80 vol.%), subordinate plagioclase (11 vol.%), and rarely, clinopyroxene. Accessory minerals (~5 vol.%) include zircon, apatite, magnetite, titanite and rutile. The subhedral, commonly cracked, 1–5 mm sized amphibole occurs as mafic crystal clots enclosing anhedral clinopyroxene crystals, biotite, magnetite and titanite. (Fig. 3c).

The studied syenite is alkaline and peraluminous with an agpaitic index of 0.64, slightly Si-undersaturated with 3.4% nepheline in the norm, and does not contain normative quartz or leucite. Sodium and potassium concentrations are high and nearly equal (6.1 wt.% $Na_2O$ and 6.2 wt.% $K_2O$; Table 2). The syenite is relatively enriched in Zr, Nb, Sr, Ba, La and Ce. Chondrite-normalised REE patterns are enriched in LREE and show a slight depletion in MREE.

*4.4. Nepheline syenite*

The white to reddish nepheline syenite is coarse- to medium-grained. It consists of large crystals of 40–55 vol% feldspar (orthoclase, microcline and subordinate albite) and 10–35 vol.% nepheline (up to 25 mm and 15 mm, respectively), subordinate biotite (2–10 vol.%) and clinopyroxene (2–7 vol.%), amphibole (2–5 vol.%), late-stage hydrothermal calcite+canrinite+sodalite+analcime and 3–5 vol.% accessory zircon, monazite, apatite, titanite, magnetite and ilmenite (Fig. 3d).

The Ditrău nepheline syenites are characterised as peraluminous and miaskitic rocks (agpaitic index varies from 0.8 to 1.0) and two different geochemical compositions are observed (Table 2). Generally, nepheline syenite-I has higher $Al_2O_3$ contents (21–24 wt.%) and alkalis (14–16 wt.% $Na_2O+K_2O$) but lower REE concentrations with a significant negative Sm anomaly than that of nepheline syenite-II ($Al_2O_3$ <21 wt.% and $Na_2O+K_2O$ <13.5 wt.%). Chondrite-normalised REE patterns of both types are U-shaped with a marked depletion in MREE typical of phonolitc compositions but MREE depletion of nepheline syenite-I is more pronounced. Both types of nepheline syenites have pronounced positive Sr and Zr-Hf anomalies and lack Eu anomalies on primitive mantle-normalised plots.

*4.5. Camptonite*

Camptonite dykes were previously investigated by Batki et al. (2004, 2014). Based on their results the clinopyroxene-bearing camptonite dykes are fine grained with a hypocrystalline porphyritic and panidiomorphic texture. Major minerals are clinopyroxene, amphibole, biotite and plagioclase. Texturally, subhedral to anhedral clinopyroxene crystals (ca. 1–10 vol.%) are set in a groundmass of kaersutite, subordinate annite, anhedral plagioclase, accessory acicular apatite, opaque minerals and titanite (Fig. 3e).

The Ditrău camptonites are basanitic and trachy-basaltic in composition and Si-undersaturated with olivine and nepheline in the norms. The samples are high in alkalis ($Na_2O/K_2O$ = 1–3) and titanium (up to 4 wt.% $TiO_2$). Mg# varies from 0.44 to 0.70 and positively correlates with Cr and Ni abundances (Table 2). High $^{143}Nd/^{144}Nd$ ratios, high field strength element (HFSE; such as Zr, Hf and Nb), large ion lithophile element (LILE; like Rb, Ba and Sr) and LREE concentrations are characteristic. Chondrite-normalised REE patterns lack Eu anomalies and show significant fractionation of HREE (La/Yb=15–38) (Batki et al., 2004, 2014).

*4.6. Tinguaite*

As noted by Batki and Pál-Molnár (2011) tinguaite dykes are fine grained with a porphyritic and sugary texture. The rocks possess clinopyroxene crystals (up to 5 vol.%) embedded in a holocrystalline to hypocrystalline groundmass where alkali feldspar randomly crosses nepheline giving a radial appearance (Fig. 3f, g). The groundmass also includes biotite microcrysts and interstitial cancrinite with accessory zircon, titanite and magnetite. Secondary biotite also occurs together with subordinate chlorite, epidote, magnetite and calcite, seldom clearly reflecting the shape of clinopyroxene crystals.

The Ditrău tinguaites are moderately to strongly silica-undersaturated (Ne=7–25) intermediate rocks (54–58 wt.% $SiO_2$) and are phonolitic in composition. They have peralkaline to peraluminous characteristics and are enriched in alkalis, Zr, Nb, Rb, Ba, Sr and LREE (Table 2). Chondrite-normalised REE patterns are convex-downwards with marked enrichment in LREE and slight enrichment in HREE (La/Yb=24–40) (Batki and Pál-Molnár, 2011).

*4.7. Ijolite*

Ijolite enclaves are holocrystalline to hypocrystalline with porphyritic textures. Major minerals are similar to tinguaites, however, mafic minerals dominate over feldspars and feldspathoids. Pale brown and green clinopyroxene crystals (up to 15 vol.%) are set in a very fine grained groundmass composed of mostly aegirine-augite needles and small biotite grains of 10–80 µm with interstitial alkali feldspar and cancrinite (Fig. 3h). Accessory minerals include titanite, apatite and magnetite. A characteristic feature of the ijolite enclaves is the presence of abundant spherical or ellipsoidal leucocratic globules, 0.2–2.0 mm in size. They contain alkali feldspar and cancrinite ± albite (Batki et al., 2012a, b).

The ijolite enclaves are nephelinitic in composition (45–49 wt.% $SiO_2$ and 11–13 wt.% $Na_2O$+$K_2O$; Table 2). They have metaluminous to peraluminous characteristics and are high in Th, U, Nb, Zr, Rb, Ba, Sr and LREE. The Cr (48–116 ppm) and Ni (57–80 ppm) concentrations are higher compared to other ijolites worldwide (e.g., 3–8 ppm Cr and <50–70 ppm Ni, Flohr and Ross, 1989; 9 ppm Cr and 33–48 ppm Ni, Wittke and Holm, 1996). Chondrite-normalised REE patterns are sloping with marked enrichment in LREE and slight depletion in MREE resulting in a convex-downwards shape.

## 5. Analytical methods

Electron microprobe analyses (EMPA) were carried out on 20 clinopyroxene crystals from 7 polished thin section (30 µm) with a JEOL 8900 electron microprobe operated in wavelength-dispersive mode at the Fachbereich Geowissenschaften, Universität Tübingen, Germany, using a beam current of 15nA, an acceleration voltage of 15 kV, and a defocused beam diameter of 10 µm and at the Institute of Geological Sciences, University of Bern, Switzerland, using a Cameca SX-50 electron microprobe in wavelength-dispersive mode

operated at an acceleration voltage of 15 kV and a beam current of 20 nA. Counting times were 16s for peak and 8s for background measurements. Additional EMPA on 7 clinopyroxene crystals from 2 polished thin sections were performed at the Institute for Geological and Geochemical Research, Research Centre for Astronomy and Earth Sciences, Hungarian Academy of Sciences, Budapest, Hungary, using a JEOL Superprobe 733 operated at an acceleration voltage of 20 kV and a beam current of 15 nA. Standards used were both natural and synthetic mineral phases. The raw data were processed using the JEOL integrated ZAF correction (Armstrong, 1991) and online PAP Cameca Software.

Trace and rare earth element concentrations in clinopyroxenes were determined by laser-ablation inductively coupled plasma mass spectrometry (LA-ICP-MS) using the same 30 µm-thick polished sections as for the EMPA and a New Wave Research UP213 Nd-YAG 213 nm UV laser system coupled to a Thermo X Series 2 ICP-MS system at Cardiff University, UK. All measurements were carried out using spot analysis and Thermo Elemental PlasmaLab time-resolved analysis mode. The laser beam diameter was 40 µm, with a frequency of 10 Hz and a power of ~5 J $cm^{-2}$. Ablations were carried out under a pure helium atmosphere. Acquisitions lasted 50 s, including a 20-s gas blank prior to laser ablation and a 10-s washout at the end. BIR-1, BIR-2, BHVO, BHVO-2, BCR and BCR2 standards were used as external standards. Ca and Si concentrations were used as internal standards to correct concentration values. Ca and Si concentrations were quantitatively measured prior to LA-ICP-MS using EPM. Gas blank subtraction and internal standard corrections were performed using Thermo Plasmalab software.

## 6. Clinopyroxene texture and zoning

Clinopyroxene crystals in the different Ditrău rocks show diverse textural and zoning features (Figs. 3 and 4) and this section describes clinopyroxene characteristics from each studied rock type.

In the poikilitic olivine-bearing cumulates, clinopyroxene microcrysts are euhedral-subhedral, unzoned, brown coloured and 150–600 µm sized (Fig. 2b in Pál-Molnár et al., 2015b). Brown clinopyroxene crystals in the pyroxene-rich cumulates are rarely zoned, euhedral to subhedral in shape and occur as macrocrysts up to 4 mm in size (Fig. 3a) (Pál-Molnár et al., 2015b).

The diorite clinopyroxene crystals are green, up to 2.7 mm in size, have an anhedral shape and are partly decomposed to chlorite and actinolite. They usually contain apatite, magnetite, titanite and hornblende inclusions (Fig. 3b).

Clinopyroxene crystals (660–800 µm) and crystal relicts (80–150 µm) in syenite are green, anhedral and partly decomposed to secondary amphibole. All the clinopyroxene crystals are enclosed by subhedral hornblende grains and occur together as crystal clots with irregular boundaries (Fig. 3c).

In the nepheline syenite, clinopyroxene is present as dark green, subhedral, elongated aegirine and aegirine-augite showing irregular zoning commonly surrounded by a magnetite + albite + biotite corona. Aegirine needles can reach 6 mm in size (Fig. 3d).

The pale brown clinopyroxene crystals in camptonites are subhedral, unzoned and 0.6- to 2.4-mm-diameter sized (Fig. 3e). They vary in abundance and generally have been replaced by an assemblage of tremolite to actinolite, and biotite (Fig. 3a in Batki et al., 2014).

In the tinguaite dykes, three clinopyroxene populations are present: 1) pale green-yellowish green crystals, 2) pale brown-beige macro- and microcrysts (0.3–1.2 mm) and 3) green groundmass microlites of 20–200 µm size. Green crystals are subhedral and show multiple zoning with an anhedral corroded core surrounded by a growth zone and a rim which usually consists of small clinoproxene grains similar to those of the green groundmass microlites (Figs. 3f and 4a, b). Pale brown clinopyroxene macro- and microcrysts are subhedral and normal zoned with an unzoned, slightly rounded core overgrown by a rim consisting of small crystals like those of the green groundmass microlites (Figs. 3g and 4c).

The ijolite enclaves consist of green clinopyroxene crystals (70–1700 µm) that are zoned, euhedral to subhedral, often skeletal enclosing the groundmass and also enclose titanite and F-apatite grains (Fig. 4d). Pale brown clinopyroxene crystal cores (50–1200 µm) show oscillatory or sector zoning. They are subhedral with slightly resorbed cores reflecting partial dissolution and are overgrown by a later aegirine-augite rim (Fig. 4e, f).

## 7. Clinopyroxene compositions

### *7.1. Major elements*

Representative major element analyses of the clinopyroxene populations can be found in Table 3 and the complete dataset is given in Supplementary Table I. In the pyroxene quadrileratal (Morimoto et al., 1989) they range in composition from diopside to aegirine-augite. The clinopyroxene compositional trends observed in the different rock types are shown in Fig. 5.

The most primitive, diopside-rich pyroxene is found in camptonite ($Di_{77–93}$, $Hd_{1–19}$, mg#=Mg/(Mg+$Fe^{2+}$)=0.81–0.99), in olivine-bearing hornblendite ($Di_{72–81}$, $Hd_{13–25}$, mg#=0.75–0.86; Pál-Molnár et al., 2015b) and in ijolite as resorbed cores ($Di_{80–94}$, $Hd_{1–15}$, mg#=0.84–0.99) (Fig. 4.e, f). In tinguaite, the growth zones around the anhedral green crystal cores (Fig. 4a, b) also have a high Di component ($Di_{78}$, mg#=0.82–0.83). Clinopyroxene in pyroxene-rich hornblendite is less primitive with higher in Hd-contents ($Di_{67–78}$, $Hd_{15–26}$, mg#=0.74–0.84), and overlaps the compositional range of camptonite crystals.

In diorite and syenite, green clinopyroxene crystals show an increase in Aeg-contents (up to 14 mol% and 43 mol%, respectively) without any significant enrichment of the Hd component (Hd<29 mol%, $mg\#_{diorite}$=0.74–0.84, $mg\#_{syenite}$=0.69–0.79) compared to hornblendite diopsides. Intermediate compositions are also represented by green clinopyroxenes from the tinguaite dykes and associated ijolite enclaves. In tinguaite, green crystal cores have hedenbergite and aegirine contents of $Hd_{20-32}Aeg_{12-15}$ (mg#=0.65–0.78), whilst in ijolite, green crystal cores span a wider compositional range (mg#=0.55–0.81) starting with high Hd up to 40 mol% and 10–23 mol% Aeg.

A similarly broad compositional range is covered by the ijolite pyroxene rims where green crystal rims ($Hd_{23-31}Aeg_{28-51}$, mg#=0.40–64) and overgrowth rims on brown resorbed cores ($Hd_{12-28}Aeg_{35-55}$, mg#=0.53–0.78) clearly overlap. Tinguaite pyroxene rims are higher both in Hd ($Hd_{26–37}$, mg#=0.19–48) and Aeg components (45–64 mol%). Continuous Aeg enrichment can be observed from ijolite pyroxene rims through ijolite ocelli ($Aeg_{43–59}$) and groundmass microlites ($Aeg_{61–63}$), tinguaite pyroxene rims to tinguaite matrix microlites ($Aeg_{69–85}$) and nepheline syenite phenocryst compositions. Nepheline syenite contains the most evolved clinopyroxene with 76–90 mol% Aeg.

Compared with trends from other alkaline suites (Fig. 5), the Ditrău pyroxenes are compositionally similar to the Lovozero (Korobeinikov and Laajoki, 1994), Alnö (Hode Vuorinen et al., 2005) and Uganda (Taylor and King, 1967) trends in that they start with a high Di-content and show a slight initial increase of $Fe^{2+}$ during fractionation before trending towards Aeg. Ijolite pyroxenes also display similarities with the Fen acmitic trend (Mitchell, 1980) indicating a notable increase in $Na^{+}$ within individual grains.

Di-rich pyroxenes in camptonite, ijolite and tinguaite are also high in $TiO_2$ (up to 3.3 wt.%, 2.3 wt.% and 3.5 wt.% respectively) and $Al_2O_3$ (up to 7.9 wt.%, 6.8 wt.% and 8.6 wt.% respectively), whilst nepheline syenite aegirine-augite ($TiO_2$ < 0.8 wt.%; $Al_2O_3$ < 2.5 wt.%) and tinguaite groundmass microlite ($TiO_2$ < 0.2 wt.%; $Al_2O_3$ < 2.2 wt.%) are poor in these elements (Fig. 6). All rim and groundmass compositions in ijolite and rims in tinguaite have low and fairly constant $Al_2O_3$ but variable $TiO_2$ contents. Green crystals in ijolite and tinguaite, and the other pyroxenes in horblendite, diorite and syenite show variable concentrations both in $TiO_2$ and $Al_2O_3$ (Fig. 6). Plots of $SiO_2$ and $Al_2O_3$ against Mg# clearly reveal two variation trends in clinopyroxene compositions. On the one hand, $SiO_2$ in brown-coloured pyroxenes increases with decreasing Mg# from camptonite and ijolite to hornblendite cumulate crystals, while $Al_2O_3$ decreases. On the other hand, the green pyroxene rims and groundmass microlites in ijolite and tinguaite show increasing $SiO_2$ and decreasing $Al_2O_3$ with decreasing Mg#. Diorite and syenite pyroxenes represent a distinct group between the two variation trends with mid-range $SiO_2$ and low $Al_2O_3$ contents (Fig. 6).

*7.2. Trace elements*

The different clinopyroxene populations, macrocryst, microphenocryst and crystal cores in the Ditrău rocks have been analysed for trace elements. However, overgrowth mantles and rims, as well as groundmass microlites, were too small to get reliable data sets by spot analyses. The analyses are summerised in Table 4 and in Supplementary Table II. Rare earth element (REE) and trace element patterns are normalised to chondritic values of McDonough and Sun (1995).

Di-rich pyroxenes in camptonite, olivine-bearing hornblendite and ijolite display variable Cr concentrations and can reach exceptionally high values up to 5540 ppm (Batki et al., 2014), 5360 ppm and 5290 ppm, respectively. In ijolite, some of the overgrowth rims which are very close to the pale brown, resorbed crystal margin (< 1847 ppm Cr) and ocelli groundmass microlite (< 1505 ppm Cr) also have high Cr contents. All the other pyroxenes have low Cr values (< 90 ppm). Zr concentrations in pyroxenes increase from primitive diopside to the most evolved aegirine-augite reaching 6260 ppm in nepheline syenite phenocryst. Generally, the increase in Aeg component accompanied by an increase in Zr is already known from other alkaline complexes (e.g. Larsen, 1976; Nielsen, 1979; Mann et al., 2006).

Normalised REE concentrations for Di-rich pyroxenes in camptonite and ijolite are 2 and 2.5 to 40 and 60 times enriched relative to chondritic values, respectively (Fig. 7a). Although resorbed crystals in ijolite are slightly more enriched in REE than camptonite macrocrysts, their patterns clearly overlap. $La_N/Yb_N$ values span a narrow range between 0.5–0.6 (camptonite macrocrysts) and between 0.6–0.9 (ijolite resorbed crystals). The REE contents of tinguaite brown pyroxene crystals are 5 to 70 times those of chondrite whilst hornblendite cumulus crystals are up to 100 times enriched relative to chondritic values (Fig. 7b). Tinguaite brown pyroxene and hornblendite pyroxene crystals have $La_N/Yb_N$ ratios of 0.8 to 1.0 and 0.7

to 1.0, respectively. Normalised REE patterns of tinguaite brown pyroxene crystals are fairly parallel to the cumulate crystals from pyroxene-rich hornblenite (Fig. 7b). The normailsed REE patterns of cumulate crystals from olivine-bearing hornblendites are very similar to camptonite and ijolite diopsides with $La_N/Yb_N$ ratios ranging between 0.4 and 0.8. All REE patterns for Di-rich pyroxenes are convex-upwards and lack a negative Eu anomaly (Fig. 7). Normalised trace element patterns for all primitive diopsides are very similar, with marked negative Pb and Ba anomalies and smaller negative anomalies for Sr and Zr. A negative Ti anomaly is also observed for all rock types except for the camptonite diopsides.

Chondrite-normalised REE patterns for Na-rich diopsides and aegirine-augites in diorite, syenite, tinguaite, ijolite and nepheline syenite are markedly variable (Fig. 8). They are enriched in both LREE and HREE but poor in MREE which results in U-shape, convex-downwards patterns, similar to those of aegirines from Puklen and Ilímaussaq (Larsen, 1976; Shearer and Larsen, 1994; Marks et al., 2004), Mont Saint-Hilaire (Piilonen at al., 1998) and Alnö (Hode Vuorinen et al., 2005). Ijolite green pyroxenes have the highest LREE concentrations (540 times chondrite) with $La_N/Yb_N$ ratios between 2.2 and 4.3 and pyroxene phenocrysts in nepheline syenite have the most pronounced enrichment of HREE (140 times chondrite) amongst Aeg component enriched pyroxenes with $La_N/Yb_N$ ratios between 1.1 and 1.9 (Fig. 8a). Syenite pyroxenes display a slight negative Eu anomaly (Eu/Eu*=0.68–0.86) whilst the other pyroxenes lack a Eu anomaly (Fig. 8b). $La_N/Yb_N$ ratios are similar to those of ijolite green pyroxenes with ranges of 2.2 to 3.0 in diorite pyroxenes, from 2.1 to 4.7 in syenite pyroxenes and from 1.8 to 3.0 in tinguaite green pyroxenes. Negative anomalies are observed for Pb, Sr, Ba and Ti similar to Di-rich pyroxenes (with the exception of pyroxenes from diorite) (Fig. 8a, b). In contrast to the Di-rich pyroxenes, the nepheline syenite clinopyroxene phenocrysts are markedly enriched in Zr and Hf (up to 6260 ppm and 184 ppm,

respectively; Fig. 9). A positive correlation exists between Hf and Sm, Sr and Ce and Yb and Zr in the Ditrău clinopyroxenes which is also observed in other pyroxene suites (e.g., Akinin et al., 2005). La/Nd and Sm/Yb ratios, the variation in Yb and Zr as well as in Hf and Sm confirm the presence of the two variation trends in clinopyroxene compositions and show that diorite and syenite pyroxenes belong to the green pyroxene compositional trend, a feature which cannot be recognised on the basis of major element compositions (Fig. 9).

## 8. Discussion

Major and trace element concentrations of the studied clinopyroxenes showing a wide range of textures and zoning patterns, reveal three compositional types of pyroxenes in the Ditrău Alkaline Massif (Figs. 5–8):

1. Pale brown, primitive ferroan, aluminian-ferroan and chromian diopsides occurring in hornblendite cumulates, camptonite and tinguaite dykes, and ijolite enclaves.
2. Green, intermediate pyroxene crystals (sodian-ferroan diopside and sodian-magnesian hedenbergite) found in diorite, syenite, ijolite and tinguaite.
3. The most evolved pyroxenes are green to dark green coloured aegirine and aegirine-augite phenocrysts in nepheline syenite as well as crystal rims and groundmass microlites in tinguaite and ijolite.

The main features of the Ditrău clinopyroxene crystals are summarised in Fig. 10. This figure also includes interpretations concerning the origin and magmatic history of the Massif that are discussed in detail below.

### *8.1. Origin of the primitive diopside crystals (Type 1)*

Primitive diopside crystals were previously described as phenocryst ( sensu stricto) phases in the Ditrău camptonites (Fig. 10a) by Batki et al. (2014) and as cumulate micro- and

macrocrysts in the Ditrău hornblendites (Fig. 10b, c) by Pál-Molnár et al. (2015b). The term 'phenocryst' is used to phases which are in equilibrium with the host melt (e.g., Cox et al., 1979; Streck, 2008), whilst 'antecrysts' are defined as crystals did not crystallise directly from the magma in which they are now hosted but represent crystals recycled by other magmas related to the same magmatic system (e.g., Charlier et al., 2005; Davidson et al., 2007; Streck, 2008; Francalanci et al., 2012; Ubide et al., 2012, 2014a, b). In tinguaite and ijolite, the partially resorbed appearance of the crystal cores in the pale brown macro- and microcrysts (Figs. 4c, e, f and 10e, g) and their similar major and trace element compositions to those of the studied camptonite diopsides (Figs. 5–7) suggest an antecrystal origin for these diopside crystals in tinguaite and ijolite. The nearly parallel trace element patterns for all the primitive Ditrău diopside populations (Fig. 7) imply that they represent co-genetic and possibly co-magmatic crystallisation sequences.

To calculate the trace element compositions of the melt in equilibrium with the primitive diopside crystals we used clinopyroxene-melt equilibrium equations with Kd values determined for camptonite compositions (Ubide et al., 2014a). Melts in equilibrium with diopside crystals in camptonite, ijolite, tinguaite and hornblendite cumulates have similar LREE, Ta and Sr enrichment and negative Pb and Zr-Hf anomalies (Fig. 11); however, they show variable REE and incompatible trace element concentrations in the different rock types. Chondrite-normalised trace element patterns for the calculated diopside equilibrium melt in camptonite and olivine-bearing hornblendite are characterised by relatively high LREE (50 to 150 and 70 to 200 times higher than C1 values, respectively) and variable Th and U concentrations (Fig. 11a–d). Melts in equilibrium with diopside in ijolite have somewhat higher LREE contents (80–300 times those of C1 values) than those of the camptonite diopside liquids (Fig. 11e,f), whilst diopside equilibrium melts in tinguaite and pyroxene-rich

hornblendite are the most enriched in REE (200–350 and 200–500 times LREE relative to C1 values, repectively) and incompatible trace elements (Fig. 11c, d, g, h).

Ditrău camptonite whole-rock compositions are also shown for comparison in Fig. 11. The calculated equilibrium melts for camptonite diopsides show essentially the same patterns as that of the whole-rock composition but the calculated melts have much lower REE and incompatible trace element concentrations than the average Ditrău camptonite magmas (Fig. 11a, b). This suggests that (i) the studied camptonite diopsides crystallised from the host camptonitic melt which points to their phenocryst s.s. origin as described previously by Batki et al. (2014), and that (ii) they represent an earlier and more primitive lamprophyric melt than those of the Ditrău camptonite magmas.

Trace element patterns and concentrations for calculated diopside equilibrium melts in olivine-bearing hornblendites are very similar to the calculated camptonite diopside liquids (Fig. 11c, d) which implies a common origin, i.e., they crystallised from the same early camptonitic melt. On the other hand, equilibrium melts calculated for diopside in pyroxene-rich hornblendite cumulate display similar trace element patterns to those of the average bulk composition of camptonite dykes indicating that these cumulus pyroxenes are likely to have been formed from more differentiated lamprophyric melts which repeatedly fed the camptonite dykes. This is in a good agreement with proposed models for the origin of the Ditrău hornblendite cumulates (Pál-Molnár et al., 2015b).

Calculated equilibrium melts for primitive diopsides occurring in ijolite and tinguaite also show similar trace element patterns to those of the camptonite bulk rock compositions but not to those of the ijolite and tinguaite whole-rock compositions (Fig. 11e–h). However, the

calculated melts have lower trace element concentrations than the camptonite melts which again suggests their origin from early lamprophyric melts. This is also consistent with the textural observations and confirms the antecrystal origin of the primitive diopside crystals in tinguaite dykes and ijolite enclaves.

*8.2. Origin of the intermediate pyroxene crystals (Type 2)*

Green clinopyroxenes have been described from many localities worldwide, for example from alkaline basalts of the Massif Central (Wass, 1979) and the Eifel region (Duda and Schmincke, 1985); from basanites of the Pannonian Basin (Dobosi and Fodor, 1992), alkaline lamprophyres of the Kola Peninsula and the Kaiserstuhl province (Arzamastsev et al., 2009); ijolites of Alnö Island (Hode Vuorinen et al., 2005) or volcanic rocks of the Leucite Hills (Barton and van Bergen, 1981) and Uganda (Taylor and King, 1967; Lloyd, 1981). These studies from different provinces suggest that green clinopyroxenes (with Mg# ranging from 0.42 to 0.77) have crystallised from evolved magmas which later mixed with a more mafic host magma or may be xenocrysts from igneous wall-rocks, or root zones of alkaline intrusions or even from the locally metasomatised upper mantle.

The studied green intermediate pyroxenes in diorite and syenite (Fig. 10h) represent anhedral, partly decomposed macrocrysts. In ijolite, these pyroxenes are euhedral to subhedral, unzoned and often skeletal (Figs. 4d and 10d), whilst in tinguaite, they appear as multiple-zoned crystals (Figs. 4a, b and 10f). Despite the textural differences, all the intermediate pyroxenes have similar major element compositions with high iron and sodium contents (Fig. 5) and similar trace element patterns (Fig. 8). To identify the equilibrium melts for intermediate pyroxenes clinopyroxene-melt equilibrium calculations were carried out using minimum and maximum mineral-melt partition coefficients determined for syenite compositions (Marks et

al., 2004). To obtain the REE concentrations of the calculated melts more specific augite-melt REE partition coefficients (Marks et al., 2004) were used.

REE patterns for the intermediate pyroxene equilibrium melts show an enrichment both in LREE and HREE relative to MREE (Fig. 12). Trace element patterns for the calculated melts have primitive mantle normalised peaks in La-Ce, Sr and Zr-Hf, along with negative Ta and Pb anomalies, and Sm-Tb depletion. Calculated Th and U concentrations are highly variable for all the equilibrium melts.

The calculated liquids for clinopyroxenes in diorite show the lowest REE compositions (100 times LREE relative to C1 values) among all calculated melts and, except for Ta, similar patterns to those of the nepheline syenite-I bulk compositons. The completely different patterns of the calculated melts for clinopyroxene from diorite to that of the diorite whole-rock composition, in accordance with textural observations, indicate that these pyroxene crystals are antecrysts and most likely originated from a Na-rich magma from which group I of the Ditrău nepheline syenitic rocks were also crystallised (Fig. 12a, b), then in the later stages of the magmatic system, these were incorporated into the dioritic magma.

Normalised trace element patterns of the calculated melts for syenite clinopyroxene cores display higher REE concentrations (200–300 times LREE relative to C1 values) and, unlike the calculated diorite pyroxene melts, they lack a positive Sr peak. Calculated melt for the syenite pyroxene rim has a marked negative Ta peak, lower MREEs and higher Th and U contents than the calculated melts in equilibrium with pyroxene cores. All the calculated syenite pyroxene melts possess similar patterns to those of the nepheline syenite-I whole-rock

compositons and not to the syenite bulk composition (Fig. 12c, d) which is consistent with an antecryst origin, like diorite clinopyroxenes.

Ijolite pyroxene equilibrium melts are more enriched in LREE (350–1400 times higher than C1 values) and other incompatible trace elements (e.g., Nb, Sr, Zr and Hf) compared to syenite pyroxene equilibrium melts. Calculated melts are similar to both ijolite and the more evolved nepheline syenite-II bulk rock composition but have slightly higher LREE and lower MREE concentrations than that of the ijolite whole-rock composition (Fig. 12e, f). However, ijolite enclaves contain numerous primitive diopside antecrysts which can modify the bulk rock composition (e.g., Ubide et al., 2014b). The Ditrău ijolite enclaves have much higher Cr concentrations than an ijolite should possess, and it is most likely that these are composed of the primitive diopside antecrysts. Thus, taking into account the skeletal texture of the ijolite intermediate pyroxene (Fig. 4d) and the similarity between calculated pyroxene melts and ijolite bulk rock compositions, we conclude that the green Na-, Nb- and Zr-rich diopside-hedenbergite population is in equilibrium with the host rock and interpret them as phenocrysts (s.s.) in ijolites. This is consistent with a magmatic origin for the green clinopyroxenes and it is likely they represent crystallisation from evolved melts (e.g., basanites of the Pannonian Basin, Dobosi and Fodor, 1992).

In tinguaite, calculated melts for the anhedral rounded cores of multiplyzoned crystals (Fig. 4a, b) have very similar trace element patterns to those of the ijolite phenocryst liquids with LREE chondrite-normalised concentrations of up to 350 (Fig. 12g, h). Positive anomalies in Th and U are notable (17,000 and 11,700 times those of C1 values, respectively). Calculated pyroxene equilibrium melts for the anhedral cores also show a good agreement with nepheline syenite-II bulk rock composition rather than with the tinguaite bulk rock composition. The

rounded nature of the cores and the calculated melt patterns together suggest an antecrystic origin for the green pyroxene cores. The calculated liquids fit best to the ijolite phenocryst pyroxene melt patterns suggesting a similar origin.

*8.3. Origin of the evolved pyroxene crystals (Type 3)*

The studied Na-rich pyroxenes in nepheline syenite are subhedral and show irregular zoning (Fig. 10i). Calculated equilibrium melts for these crystals have a marked U-shaped patterns with high LREE and HREE concentrations (150–300 times LREE and 70 times HREE relative to C1 values) (Fig. 12i, j). They also have a marked enrichment in Th, U, Nb and Zr-Hf. With the exception of HREE, Th, U, Nb and Zr-Hf, the calculated melts for aegirine-augites are similar to nepheline syenite-II bulk rock composition confirming the phenocryst s.s. origin of these pyroxene crystals as previously proposed by Morogan et al. (2000), Fall et al. (2007) and Pál-Molnár (2010b).

HREE enrichment is also observed in sodic-calcic and particularly Na-rich mafic silicates, for example in the Grønnedal-Ika aegirine-augites and the Puklen and Ilímaussaq aegirines. It is interpreted to be due to a crystal chemical control on trace element partitioning (Marks et al., 2004). REE enrichment in sodic-calcic clinopyroxenes towards sodic members may reflect a general preference for $3^+$ REE as the incorporation of $Na^+$ needs charge balance with a trivalent ion ($Na^+ + REE^{3+} \leftrightarrow 2\ Ca^{2+}$ on the M2 site) as proposed by Wood and Blundy (1997) . This partitioning in clinopyroxene should also affect the LREE abundances, which is confirmed by the LREE enrichment in the Ditrău aegirine-augites. A pronounced enrichment in Zr and Hf with increasing Na-content can also be observed.

Calculated equilibrium melt for the tinguaite green pyroxene rims are similar to the nepheline syenite aegirine-augite crystals with 600 times LREE and 40 times HREE relative to C1 values, and a particularly high Zr-Hf peak (3,900 and 1,700 times those of C1 values, respectively) inferring crystallisation from the same phonolitic melt as aegirine-augite phenocrysts (Fig. 12g–j).

*8.4. Fractionation and accumulation*

The overall similar trace element patterns for all the calculated primitive diopside equilibrium melts and the bulk rock composition of the Ditrău camptonite dykes (Fig. 11) indicate that the Fe-diopside crystals and the camptonite dykes originate from basanitic parental melts (called magma1) from the same magmatic environment (Fig. 13). Slight differences in trace element distributions of the equilibrium melts suggest that the primitive diopside populations observed in camptonite, hornblendite, tinguaite and ijolite could have derived from multiple recharge events of magma1 (M1) and reflect different stages of the evolution of the parental basanitic melts which have already undergone fractional crystallisation at deeper levels (e.g., Furman et al., 1992; Weidendorfer et al., 2014). Fe-diopside phenocrysts s.s. of the camptonite sample VRG7292 most probably represent the earliest stage of evolution. The early camptonitic magma has undergone small-to-moderate degrees of closed-system fractional crystallisation (modelled maximum degree of fractionation [$F_{max}$] = 46.8; Batki et al., 2014) producing differentiated mafic magmas, called magma1a (M1a) (Fig. 13b). Further fractional crystallisation and crystal accumulation has taken place (Pál-Molnár et al., 2015b) generating cumulus pyroxene macrocrysts in the pyroxene-rich hornblendite cumulates (Fig. 13b). Cumulus pyroxene microcrysts in olivine-bearing hornblendite cumulates are also the result of closed-system processes, however, these crystallised and accumulated directly from the early camptonitic magma (M1) (Fig. 13a).

*8.5. Magma recharge, crystal recycling and mingling*

Mineral textures and compositions preserve changes in magmatic systems. Interactions of discrete magma batches can result in disequilibrium features such as mineral dissolution and overgrowth rims on pre-existing crystals (Streck, 2008). In the following section we discuss the observed clinopyroxene textures and compositions to identify the open-system processes of magma recharge, crystal recycling and mingling. The term 'mingling' is used in the sense of mechanical interaction and physical dispersion among two magmas (e.g., Barbarin and Didier, 1992; Michel et al., 2016).

Major and trace element compositional variations (Figs. 5 and 8) and similarity in calculated equilibrium melt compositions for all the green intermediate pyroxenes (Fig. 12) indicate their common origin and represent a different magma source, called magma2 (M2), in the Ditrău magmatic system. This magma is represented by the ijolite clinopyroxene phenocryst s.s. phases (Fig. 13c). The primitive Fe-diopside antecrysts could have been recycled by repeated injections of M1 magma batches (recharge of magma1) into the ijolitic magmatic environment (Fig. 13c). This magma, including the green pyroxene phenocrysts and the recycled primitive diopside antecrysts, fractionated towards to the ijolitic magma composition, called magma2a, and is represented by overgrowth rims on ijolite phenocrysts and antecrysts, and ijolite groundmass microlite crystals. Further fractionation produced a phonolitic magma (called magma2b) which crystallised clinopyroxene phenocrysts s.s. of aegirine-augitic composition in nepheline syenite and aegirine-augite groundmass microlites in tinguaite (Fig. 13c).

The ijolite green clinopyroxene phenocrysts were also recycled from M2 into the M1a environment through M2 recharge events that resulted in disequilibrium textures. The

rounded, resorbed shape of the green pyroxene cores can be explained by the higher temparature of M1a which dissolved the green crystals. These are mantled by an overgrowth zone of M1a composition reflecting subsequent crystallisation in the M1a environment (Fig. 13d). A new recharge event of M1a recycled a number of these green mantled cores and primitive Fe-diopside crystals from M1a into the phonolitic magma (M2b) from which aegirine-augite crystallised as rims around both antecryst populations (Fig. 13e) followed by the formation of tinguaite groundmass microlites as indicated by their compositions (Fig. 5). The presence of rounded ijolite enclaves in tinguaite dykes (Fig. 2b) indicates that magma mingling occurred between co-existing M2a and M2b before solidification (Fig. 13f). The enclaves most likely formed by injection of the mafic M2a magma into the felsic M2b magma, i.e., the crystallising tinguaite dyke (e.g., Barbarin and Didier, 1992; Ubide et al., 2014c).

As suggested by the compositional similarity of calculated equilibrium melts for all the green intermediate pyroxenes (Fig. 12), all of these crystals derive from the Na-enriched magma2. However, equilibrium melts for diorite pyroxene antecrysts represent slighty more primitive compositions compared to those of the pyroxenes in syenite, ijolite or tinguaite. These differences in trace element distributions of the equilibrium melts suggest that the intermediate pyroxene populations observed in diorite, syenite, ijolite and tinguaite could have originated from repeated recharge events of magma2 and reflect different stages of the evolution of the parental melts. The green pyroxene antecrysts, present in diorite, could have been recycled into the dioritic magma through an M2 recharge (Fig. 13g). The presence of amphibole crystal clots including green pyroxene antecrysts in syenites (Fig. 13h) confirms repeated recharge events and crystal recycling in the magmatic evolution of the Ditrău rocks.

## 9. Conclusions

1. The texture and composition of diverse clinopyroxene populations in the Ditrău alkaline igneous rocks reveals the complexity of deep magmatic processes and the evolution history of different magmas and magma sources. The different clinopyroxene crystals show evidence for open- and closed-system petrogenetic processes that played a role in the magmatic evolution: magma recharge, pyroxene recycling through interaction of magma batches, mingling, fractional crystallisation and accumulation.
2. Clinopyroxenes record two major magma sources and evolution trends. The high-Cr Fe-diopside population derive from an early camptonitic magma (magma1) derived from basanitic parental melts, whilst the Na-Fe diopside crystals, rich in Nb and Zr, originate from another distinct magma source (magma2). Fe-diopsides show increasing Hd component and REE concentrations during fractionation of magma1. Meanwhile, in the Na-rich magmatic environment (magma2), clinopyroxenes display a continuous development from Na-diopside-hedenbergite towards aegirine-augitic compositions coupled with a pronounced HREE, Nb, Zr and Hf enrichment with increasing Na/Ca ratio.
3. Multiple interactions between the identified magma batches indicate that repeated recharge events of magma1 and magma2 resulted in crystal recycling and mingling between the co-existing magma batches. These events represent the dominant open-system petrogenetic processes that were involved in the evolution of the magmatic system.
4. Investigation of complex zoning characteristics and equilibrium melt calculations reveal a diverse antecryst cargo in the studied Ditrău rocks. Antecryst recycling into dioritic, syenitic, tinguaitic and ijolitic magma is described for the first time in the

magmatic history of the Ditrău Alkaline Massif. Incorporated crystals can significantly affect the original magma composition and therefore, whole-rock chemical data should be interpreted with great care. Hence, this study reveals that detailed mineral-scale analysis is crucial not only in reconstructions of complex subvolcanic plumbing systems but also in investigations of plutonic rocks.

**Acknowledgements**

We are grateful to Thomas Wenzel at Fachbereich Geowissenschaften, Universität Tübingen and Gábor Dobosi at the Institute for Geological and Geochemical Research, Research Centre for Astronomy and Earth Sciences, Hungarian Academy of Sciences, Budapest for their help with EMPA analyses and constructive comments on the microprobe results. Iain McDonald at Cardiff University is gratefully acknowledged for assistance with LA-ICP-MS analyses. This work was funded by the ’Vulcano’ Petrology and Geochemistry Research Group, Department of Mineralogy, Geochemistry and Petrology, University of Szeged (Hungary). Anikó Batki was supported by the Campus Hungary, National Excellence Programme co-financed by the European Union and the State of Hungary in the framework of the Social Renewal Operational Programme (TÁMOP-4.2.4B/2-11/1-2012-0001).

**References**

Akinin, V.V., Sobolev, A.V., Ntaflos, T., Richter, W., 2005. Clinopyroxene megacrysts from Enmelen melanephelinitic volcanoes (Chukchi Peninsula, Russia): application to composition and evolution of mantle melts. Contributions to Mineralogy and Petrology 150, 85–101.

Armstrong, J.T., 1991. Quantitative elemental analysis of individual microparticles with electron beam instruments, in: Heinrich, K.F.J., Newbury, D.E. (Eds.), Electron Probe Quantitation. Plenum Press, New York, pp. 261–315.

Arzamastsev, A.A., Arzamastseva, L.V., Bea, F., Montero, P., 2009. Trace elements in minerals as indicators of the evolution of alkaline ultrabasic dike series: LA-ICP-MS data for the magmatic provinces of northeastern Fennoscandia and Germany. Petrology 17/1, 46–72.

Balintoni, I., Balica, C., Ducea, H., Horst-Peter, H., 2014. Peri-Gondwanan terranes in the Romanian Carpathians: A review of their spatial distribution, origin, provenance, and evolution. Geoscience Frontiers 5/3, 395–411.

Barbarin, B., Didier, J., 1992. Genesis and evolution of mafic microgranular enclaves through various types of interaction between coexisting felsic and mafic magmas. Earth Environmental Science Transactions of the Royal Society of Edinburgh 83, 145–153.

Barton, M., van Bergen, M.J., 1981. Green clinopyroxenes and associated phases in a potassium-rich lava from the Leucite Hills, Wyoming. Contributions to Mineralogy and Petrology 77/2, 101–114.

Batki, A., Pál-Molnár, E., Bárdossy, A., 2004. Occurrence and petrology of lamprophyres from the northern part of the Ditrău Alkaline Massif, Eastern Carpathians, Romania. Acta Mineralogica Petrographica 45/2, 21–28.

Batki, A., Pál-Molnár, E., 2011. Petrology of tinguaites from the Ditrău Alkaline Massif, Romania. 9th Meeting of the Central European Tectonic Studies Group, Skalsky Dvur, Czech Republic, 2.

Batki, A., Pál-Molnár, E., Markl, G., Wenzel, T., 2012a. Compositional variations of clinopyroxene from ijolite, Ditrău Alkaline Massif, Romania. Joint 5th Mineral Sciences

in the Carpathians Conference and 3rd Central-European Mineralogical Conference, Miskolc, Hungary. Acta Mineralogica-Petrographica, Abstract Series 7, 12.

Batki, A., Pál-Molnár, E., Markl, G., Wenzel, T., 2012b. Magma mixing in ijolite from the Ditrău Alkaline Massif, Romania: Textural relations and compositional variations of mafic minerals. 1st European Mineralogical Conference, Frankfurt, Germany, 464.

Batki, A., Pál-Molnár, E., Dobosi, G., Skelton, A., 2014. Petrogenetic significance of ocellar camptonite dykes in the Ditrău Alkaline Massif, Romania. Lithos 200–201, 181–196.

Baxter, S., Feely, M., 2002. Magma mixing and mingling textures in granitoids: examples from the Galway Granite, Connemara, Ireland. Mineralogy and Petrology 76, 63–74.

Charlier, B.L.A., Wilson, C.J.N., Lowenstern, J.B., Blake, S., Van Calsteren, P.W., Davidson, J.P., 2005. Magma generation at a large, hyperactive silicic volcano (Taupo, New Zealand) revealed by U–Th and U–Pb systematics in zircons, Journal of Petrology 46 (1), 3–32.

Codarcea, A. Codarcea, D.M., Ianovici, V., 1957. Structura geologică a masivului de roci alkaline de la Ditrău. Buletin Ştiinţific, Secţia de Geologie şi Geografie II/3–4, 385–446.

Cox, K.G., Bell, J.D., Pankhurst, R.J., 1979. Petrographic aspects of volcanic rocks. In: The Interpretation of Igneous Rocks. Springer, Dordrecht.

Dallmeyer, D.R., Kräutner, H.G., Neubauer, F., 1997. Middle-late Triassic $^{40}Ar/^{39}Ar$ hornblende ages for early intrusions within the Ditrău Alkaline Massif, Rumania: Implications for Alpine rifting in the Carpathian orogen. Geologica Carpathica 48, 347–352.

Davidson, J.P., Morgan, D.J., Charlier, B.L.A., Harlou, R., Hora, J.M., 2007. Microsampling and isotopic analysis of igneous rocks: implications for the study of magmatic systems. Annual Review of Earth and Planetary Sciences 35, 273–311.

Dobosi, G., Fodor, R.V., 1992. Magma fractionation, replenishment, and mixing as inferred from green-core clinopyroxenes in Pliocene basanite, southern Slovakia. Lithos 28/2, 133–150.

Dobosi, G., Schultz-Güttler, R., Kurat, G., Kracher, A., 1991. Pyroxene chemistry and evolution of alkali basaltic rocks from Burgenland and Styria, Austria. Mineralogy and Petrology 43/4, 275–292.

Duda, A., Schmincke, H.-U., 1985. Polybaric differentiation of alkali basaltic magmas: evidence from green-core clinopyroxenes (Eifel, FRG). Contributions to Mineralogy and Petrology 91/4, 340–353.

Fall, A., Bodnar, R. J., Szabó, Cs., Pál-Molnár, E., 2007. Fluid evolution in the nepheline syenites of the Ditrău Alkaline Massif, Transylvania, Romania. Lithos 95, 331–345.

Flohr, M.J.K., Ross, M., 1989. Alkaline igneous rocks of Magnet Cove, Arkansas: Metasomatized ijolite xenoliths from Diamond Jo quarry. American Mineralogist 74, 113–131.

Francalanci, L., Avanzinelli, R., Nardini, I., Tiepolo, M., Davidson, J.P., Vannucci, R., 2012. Crystal recycling in the steady-state system of the active Stromboli volcano: a 2.5-ka story inferred from in situ Sr-isotope and trace element data. Contributions to Mineralogy and Petrology 163, 109–131.

Frost, T.P., Mahood, G.A., 1987. Field, chemical, and physical constraints on mafic–felsic magma interaction in the Lamarck Granodiorite, Sierra Nevada, California. Geological Society of America Bulletin 99, 272–291.

Furman, T., Frey, F., Meyer, P.S., 1992. Petrogenesis of evolved basalts and rhyolites at Austurhorn, southeastern Iceland: the role of fractional crystallization. Journal of Petrology 33, 1405–1445.

Gernon, T.M., Upton, B.G.J., Ugra, R., Yücel, C., Taylor, R.N., Elliott, H., 2016. Complex subvolcanic magma plumbing system of an alkali basaltic maar-diatreme volcano (Elie Ness, Fife, Scotland). Lithos 264, 70-85.

Hode Vuorinen, J., Hålenius ,U., Whitehouse, M.J., Mansfeld, J., Skelton, A.D.L., 2005. Compositional variations (major and trace element) of clinopyroxene and Ti-andradite from pyroxenite, ijolite and nepheline syenite, Alnö Island, Sweden. Lithos 81, 55–77.

Hoeck, V., Ionescu, C., Balintoni, I., Koller, F., 2009. The Eastern Carpathians "ophiolites" (Romania): remnants of a Triassic ocean. Lithos 108, 151–171.

Irvine, T.N., Baragar, W.R.A., 1971. A guide to the chemical classification of the common volcanic rocks. Canadian Journal of Earth Sciences 8, 523–548.

Jankovics, M.É., Harangi, S., Kiss, B., Ntaflos, T., 2012. Open-system evolution of the Füzes-tó alkaline basaltic magma, western Pannonian Basin: constraints from mineral textures and compositions. Lithos 140–141, 25–37.

Jankovics, M.É., Taracsák, Z., Dobosi, G., Embey-Isztin, A., Batki, A., Harangi, Sz., Hauzenberger, C.A., 2016. Clinopyroxene with diverse origins in alkaline basalts from the western Pannonian Basin: Implications from trace element characteristics. Lithos 262, 120–134.

Kerr, A.C., Kent, R.W., Thomson, B.A., Seedhouse, J.K., Donaldson, C.H., 1999. Geochemical evolution of the Tertiary Mull volcano, western Scotland. Journal of Petrology 40, 873–908.

Korobeinikov, A.N., Laajoki, K., 1994. Petrological aspects of the evolution of clinopyroxene composition in the intrusive rocks of the Lovozero alkaline massif. Geochemistry International 31, 69–76.

Kozur, H., 1991. The evolution of the Meliata-Hallstatt ocean and its significance for the early evolution of the Eastern Alps and Western Carpathians. Palaeogeography, Palaeoclimatology, Palaeoecology 87/1–4, 109–135.

Kräutner, H.G., Bindea, G., 1998. Timing of the Ditrău alkaline intrusive complex (Eastern Carpathians, Romania). Slovak Geological Magazine 4, 213–221.

Kretz, R., 1983. Symbols for rock-forming minerals. American Mineralogist 68, 277–279.

Larsen, L.M., 1976. Clinopyroxenes and coexisting mafic minerals from the alkaline Ilimaussaq intrusion, south Greenland. Journal of Petrology 17, 258–290.

Lloyd, F.E., 1981. Upper mantle metasomatism beneath the continental rift: Clinopyroxenes in alkali mafic lavas and nodules from South West Uganda. Mineralogical Magazine 44, 315–323.

Ma, X., Meert, J.G., Xu, Z., Zhao, Z., 2017. Evidence of magma mixing identified in the Early Eocene Caina pluton from the Gangdese Batholith, southern Tibet. Lithos 278–281, 126–139.

Mann, U., Marks, M., Markl, G., 2006. Influence of oxygen fugacity on mineral compositions in peralkaline melts: The Katzenbuckel volcano, Southwest Germany. Lithos 91, 262–285.

Marks, M., Halama, R., Wenzel, T., Markl, G., 2004. Trace element variations in clinopyroxene and amphibole from alkaline to peralkaline syenites and granites: implications for mineral–melt trace-element partitioning. Chemical Geology 211, 185–215.

McDonough, W.F., Sun, C.C., 1995. Composition of the Earth. Chemical Geology 120, 223–253.

Michel, L., Wenzel, T., Markl, G., 2016. Interaction between two contrasting magmas in the Albtal pluton (Schwarzwald, SW Germany): textural and mineral – chemical evidence. International Journal of Earth Science, DOI: 10.1007/s00531–016–1363–7

Mitchell, R.H., 1980. Pyroxenes of the Fen alkaline complex, Norway. American Mineralogist 65, 45–54.

Mitchell, R.H., Vladykin, N.V., 1996. Compositional variation of pyroxene and mica from the little murun ultrapotassic complex, Aldan Shield, Russia. Mineralogical Magazine 60, 907–925.

Morimoto, N., Fabries, J., Ferguson, A.K., Ginzburg, I.V., Ross, M., Seifert, F.A., Zussman, J., Aoki, K., Gottardi, G., 1989. Nomenclature of pyroxenes. Subcommittee on pyroxenes. American Mineralogist 73, 1123–1133.

Morogan, V., Upton, B.G.J., Fitton, J.G., 2000. The petrology of the Ditrău alkaline complex, Eastern Carpathians. Mineralogy and Petrology 69, 227–265.

Nakagawa, M., Wada, K., Wood, C.P., 2002. Mixed magmas, mush chambers and eruption triggers: evidence from zoned clinopyroxene phenocrysts in andesitic scoria from the 1995 eruptions of Ruapehu volcano. New Zealand. Journal of Petrology 43/12, 2279–2303.

Neumann, E.-R., Wulff-Pedersen, E., Simonsen, S.L., Pearson, N.J., Martí, J., Mitjavila, J., 1999. Evidence for fractional crystallization of periodically refilled magma chambers in Tenerife, Canary Islands. Journal of Petrology 40/7, 1089–1123.

Nielsen, T.F.D., 1979. The occurrence and formation of Ti aegirines in peralkaline syenites. Contributions to Mineralogy and Petrology 69, 236–244.

Pană, D., Balintoni, I., Heaman L., 2000. Precise U–Pb zircon dating of the syenite phase from Ditrău Alkaline Igneous Complex. Studia Universitatis Babeş-Bolyai, Geologia 45/1, 79–89.

Pál-Molnár, E., 2000. Hornblendites and diorites of the Ditrău Syenite Massif. Ed. Department of Mineralogy, Geochemistry and Petrology, University of Szeged, Szeged, 172 p.

Pál-Molnár, E., 2010a. Geology of Székelyland, in: Szakáll, S., Kristály, F. (Eds.), Mineralogy of Székelyland, Eastern Transylvania, Romania. Ed. Csík County Nature and Conservations Society, Sfântu Gheorghe–Miercurea-Ciuc–Târgu Mureș, pp. 33–43.

Pál-Molnár, E., 2010b. Rock-forming minerals of the Ditrău Alkaline Massif, in: Szakáll, S., Kristály, F. (Eds.), Mineralogy of Székelyland, Eastern Transylvania, Romania. Ed. Csík County Nature and Conservations Society, Sfântu Gheorghe–Miercurea-Ciuc–Târgu Mureș, pp. 63–88.

Pál-Molnár, E., Árva-Sós, E., 1995. K/Ar radiometric dating on rocks from the northern part of the Ditrău Syenite Massif and its petrogenetic implications. Acta Mineralogica-Pertrographica 36, 101–116.

Pál–Molnár, E., Batki, A., Ódri, Á., Kiss, B., Almási, E., 2015a. Geochemical implications fot the magma origin of granitic rocks from the Ditrau Alkaline Massif (Eastern Carpathians, Romania). Geologia Croatica 68/1, 51–66.

Pál-Molnár, E., Batki, A., Almási, E., Kiss, B., Upton, B.G.J., Markl, G., Odling, N., 2015b. Origin of mafic and ultramafic cumulates from the Ditrău Alkaline Massif, Romania. Lithos 239, 1–18.

Piilonen, P.C, Mcdonald, A.M., Lalonde, A.E., 1998. The crystal chemistry of aegirine from Mont Saint-Hilaire, Quebec. Canadian Mineralogist 36, 779–791.

Săndulescu, M., 1984. Geotectonica României. Editura Technică, Bucureşti 336 p.

Săndulescu, M., Kräutner, H.G., Balintoni, I., Russo-Săndulescu, M., Micu, M., 1981. The Structure of the East Carpathians (Moldavia – Maramures Area). Guide Exc. B1, XII

Congress of the Carpathian Balkan Geological Association, Inst. Geol. Geophys., Bucuresti, 92 p.

Shane, P., Doyle, L.R., Nairn I.A., 2008. Heterogeneous andesite-dacite ejecta in 26-16.6 ka pyroclastic deposits of Tongariro Volcano, New Zealand: the product of multiple magma-mixing events. Bulletin of Volcanology 70, 517–536.

Shearer, C.K., Larsen, L.M., 1994. Sector-zoned aegirine from the Ilimaussaq alkaline intrusion, South Greenland: implications for trace-element behaviour in pyroxene. American Mineralogist 79, 340–352.

Stephenson, D., 1972. Alkali clinopyroxenes from nepheline syenites of the South Qôroq Centre, south Greenland. Lithos 5, 187–201.

Streck, M.J., 2008. Mineral textures and zoning as evidence for open system processes, in: Putirka, K.D., Tepley, F.J., III (Eds) Minerals, Inclusions and Volcanic Processes. Mineralogical Society of America and Geochemical Society, Reviews in Mineralogy and Geochemistry 69, pp. 595–622.

Streck, M., Dungan, M., Malavassi Reagan, M., Bussy, F., 2002. The role of basalt replenishment in the generation of basaltic andesites of the ongoing activity at Arenal volcano, Costa Rica: evidence from clinopyroxene and spinel. Bulletin of Volcanology 64/5, 316–327.

Streckeisen, A., 1954. Das Nephelinsyenit-Massiv von Ditro (Siebenbürgen), II. Teil. Schweizeriche Mineralogische und Petrographische Mitteilungen 34, 336–409.

Streckeisen, A., 1960. On the structure and origin of the Nepheline-Syenite Complex of Ditro (Transsylvania, Romania). Rep. 21th IGC. 13, 228–238.

Streckeisen, A., Hunziker, J.C., 1974. On the origin of the Nephelinsyenit Massif of Ditró (Transylvania, Romania). Schweizerische Mineralogische und Petrographische Mitteilungen 54, 59–77.

Stroncik, N., Klügel, A., Hansteen, T., 2009. The magmatic plumbing system beneath El Hierro (Canary Islands): constraints fromphenocrysts and naturally quenched basaltic glasses in submarine rocks. Contribution to Mineralogy and Petrology 157/5, 593–607.

Tyler, R.C., King, B.C., 1967. The pyroxenes of the alkaline igneous complexes of Eastern Uganda. Mineralogical Magazine 280, 5–22.

Ubide, T., Arranz, E., Lago, M., Galé, C., Larrea, P., 2012. The influence of crystal settling on the compositional zoning of a thin lamprophyre sill: A multi-method approach. Lithos 132–133, 37–49.

Ubide, T., Galé, C., Arranz, E., Lago, M., Larrea, P., 2014a. Clinopyroxene and amphibole crystal populations in a lamprophyre sill from the Catalonian Coastal Ranges (NE Spain): A record of magma history and a widow to mineral-melt partitioning. Lithos 184–187, 225–242.

Ubide, T., Galé, C., Larrea, P., Arranz, E., Lago, M., 2014b. Antecrysts and their effect on rock compositions: The Cretaceous lamprophyre suite in the Catalonian Coastal Ranges (NE Spain). Lithos 206–207, 214–233.

Ubide, T., Galé, C., Larrea, P., Arranz, E., Lago, M., Tierz, P., 2014c. The relevance of crystal transfer to magma mixing: a case study in composite dykes from the Central Pyrenees. Journal of Petrology 55/8, 1535–1559.

Wass, S.Y., 1979. Multiple origins of clinopyroxenes in alkali basaltic rocks. Lithos 12(2), 115–132.

Weidendorfer, D., Mattsson, H.B., Ulmer, P., 2014. Dynamics of Magma Mixing in Partially Crystallized Magma Chambers: Textural and Petrological Constraints from the Basal Complex of the Austurhorn Intrusion (SE Iceland). Journal of Petrology 55/9, 1865–1903.

Winpenny, B., Maclennan, J., 2011. A partial record of mixing of mantle melts preserved in Icelandic phenocrysts. Journal of Petrology 52, 1791–1812.

Wittke, J.H., Holm, R.F., 1996. The association basanitic nephelinite – feldspar ijolite – nepheline monzosyenite at House Mountain volcano, North-Central Arizona. The Canadian Mineralogist 34, 221–240.

Wood, B.J., Blundy, J.D., 1997. A predictive model for rare earth element partitioning between clinopyroxene and anhydrous silicate melt. Contributions to Mineralogy and Petrology 129, 166–181.

**Figure captions**

Fig. 1. (A) Location of the Ditrău Alkaline Massif in the structural system of the Alpine Carpathian–Dinaric region (Pál-Molnár, 2010a). (B) Alpine structural units of the Eastern Carpathians (Săndulescu et al., 1981, modified). (C) Schematic geological map of the Ditrău Alkaline Massif (Pál-Molnár et al., 2015b) showing sample locations.

Fig. 2. Field relations indicating mingling features between co-existing magmas in the Ditrău Alkaline Massif. (A) Diorite enclaves enclosed in syenite at Jolotca Creek. (B) Fine-grained ijolite enclaves in tinguaite dykes at Creanga Mare Creek.

Fig. 3. Characteristic petrographic features of the studied igneous rocks containing clinopyroxene in the Ditrău Alkaline Massif. (A) Brown cumulus diopside in pyroxene-rich hornblendite cumulate VRG6706, 1N. (B) Green, anhedral clinopyroxene crystal extensively decomposed to chlorite and actinolite in diorite VRG6567, 1N. (C) Hornblende crystal clot enclosing green, anhedral clinopyroxene crystals and crystal relicts, biotite, magnetite and titanite in syenite VRG7420, 1N. (D) Dark green, subhedral aegirine-augite showing irregular zoning with magnetite+albite+biotite corona in nepheline syenite VRG6727, 1N. (E) Pale

brown, subhedral diopside crystals in ocellar camptonite dyke VRG7292, 1N. (F) Contact between ijolite enclave and the host tinguaite dyke VRG7338, 1N. (G) Fe-diopside crystals overgrown by aegirine-augite groundmass microlites in tinguaite dyke VRG7306, 1N. (H) Green, euhedral and skeletal clinopyroxene together with brown, subhedral diopside, biotite aggregates, ocelli and feldspar xenocryst in ijolite enclave VRG7338, 1N. Mineral abbreviations are after Kretz (1983).

Fig. 4. BSE images of detailed textural and zoning characteristics of the Ditrău tinguaite and ijolite clinopyroxene crystals showing the analysed laser spots. (A and B) Multiple-zoned green clinopyroxene crystals with anhedral, rounded cores, growth reverse zones and overgrowth rims similar to the groundmass microlites in tinguaite VRG7338 and VRG7306. (C) Unzoned, subhedral diopside clot overgrown by aegirine-augite in tinguaite VRG7306. (D) Green, euhedral and skeletal clinopyroxene phenocryst enclosing titanite and F-apatite in ijolite VRG7338 (note the same mineral assemblages in the skeletal parts of the crystal and the groundmass). (E and F) Brown, subhedral pyroxene crystals with sector and oscillatory zoning showing resorbed cores and overgrowth aegirine-augite rim in ijolite VRG7338.

Fig. 5. Compositional variations of the Ditrău clinopyroxenes in terms of Di–Hd–Aeg end member mol%. In the right triangle clinopyroxene trends from other alkaline complexes are shown for comparison: (1) Murun, Siberia (Mitchell and Vladykin, 1996), (2) Lovozero, Kola Peninsula (Korobeinikov and Laajoki, 1994), (3) Fen, Norway, acmitic trend (Mitchell, 1980), (4) Alnö Island, Sweden, sodic trend (Hode Vuorinen et al., 2005), (5) Eastern Uganda (Taylor and King, 1967), (6) South Qôroq, South Greenland (Stephenson, 1972), (7) Ilímaussaq, South Greenland (Larsen, 1976).

Fig. 6. Major element variation diagrams for the Ditrău clinopyroxenes with respect to Mg#. Symbol legend is the same as in Fig. 5.

Fig. 7. Chondrite-normalised REE and trace element patterns for Fe-diopsides of (A) Ditrău camptonite and ijolite and (B) Ditrău hornblendite cumulates and tinguaite dykes. Normalising values are after McDonough and Sun (1995).

Fig. 8. Chondrite-normalised REE and trace element patterns for Na-Fe diopsides of (A) Ditrău nehpehline syenite, tinguaite and ijolite and (B) Ditrău syenite, diorite and ijolite for comparison. Normalising values are after McDonough and Sun (1995).

Fig. 9. Trace element compositions and Sm/Yb vs La/Nd ratios of the Ditrău clinopyroxenes. Symbol legend is the same as in Fig. 5. except purple stars which represent Fe-diopside cores in tinguaite dykes.

Fig. 10. Summary of the Ditrău clinopyroxene textures, zoning, chemical characteristics and the interpretation in regard to their origin and crystallisation history. M1–magma1, M1a–magma1a, M2–magma2, M2a–magma2a, M2b–magma2b which refer to magmatic environments in the Ditrău Alkaline Massif.

Fig. 11. Chondrite-normalised (McDonough and Sun, 1995) REE and trace element patterns of calculated equilibrium melts for the Ditrău Fe-diopsides compared to those of the studied camptonite sample VRG7292 and the average Ditrău camptonites (Batki et al., 2014), tinguaite (sample VRG7306) and ijolite (sample VRG7338) whole-rock compositions. Ol Hbl: Olivine-bearing Hornblendite, Px Hbl: Pyroxene-rich hornblendite.

Fig. 12. Chondrite-normalised (McDonough and Sun, 1995) REE and trace element patterns of calculated equilibrium melts for the Ditrău Na-Fe diopsides and aegirine-augites compared to those of the Ditrău nepheline syenite (unpublished data except representative samples VRG7506 and VRG7507), syenite (sample VRG7420), diorite (sample VRG6774), ijolite (sample VRG7338) and tinguaite (sample VRG7306) whole-rock compositions.

Fig. 13. Schematic model of open and closed system processes involved in the magmatic evolution of the studied Ditrău rocks. Mineral symbols and abbreviations for magmatic environments are the same as in Fig. 10. except brown hexagons which represent amphibole crystals and green rectangles that represent biotite in diorite and syenite (g and h).

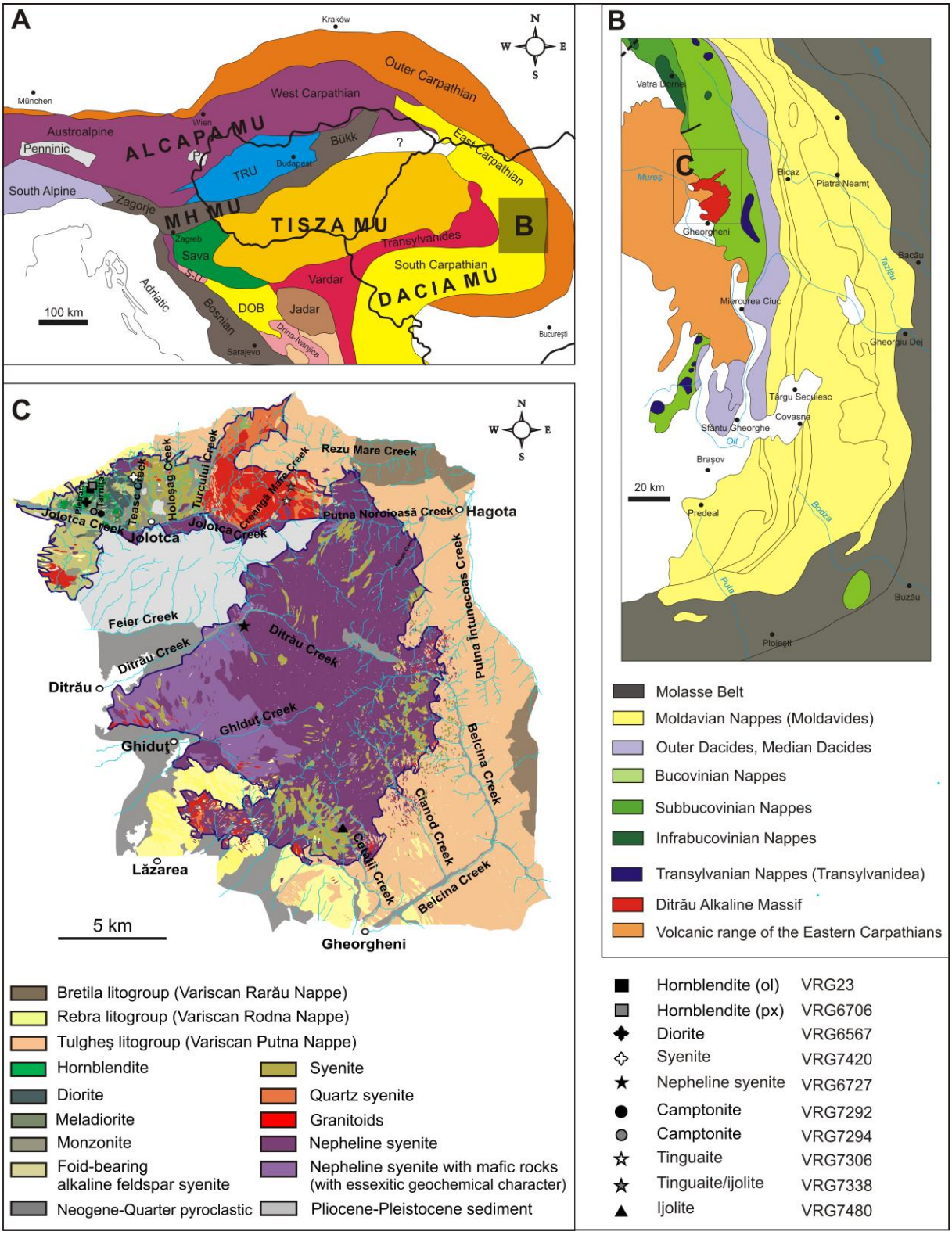


Figure 1

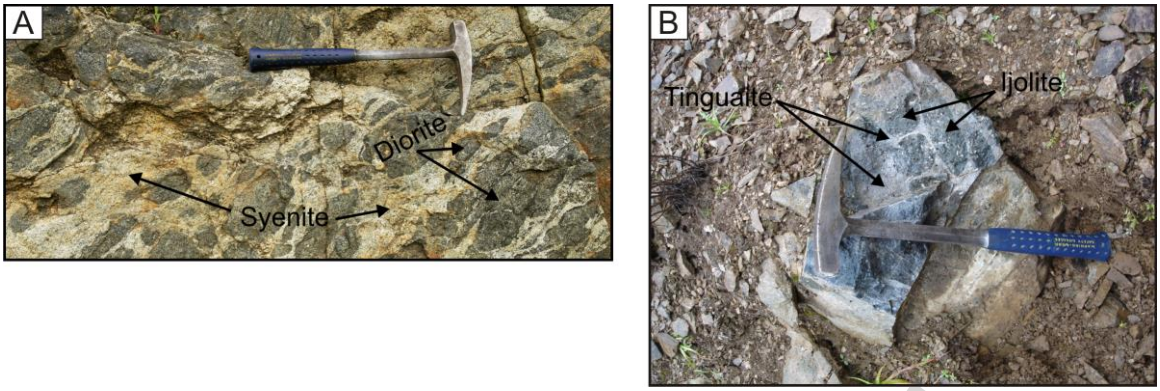


Figure 2

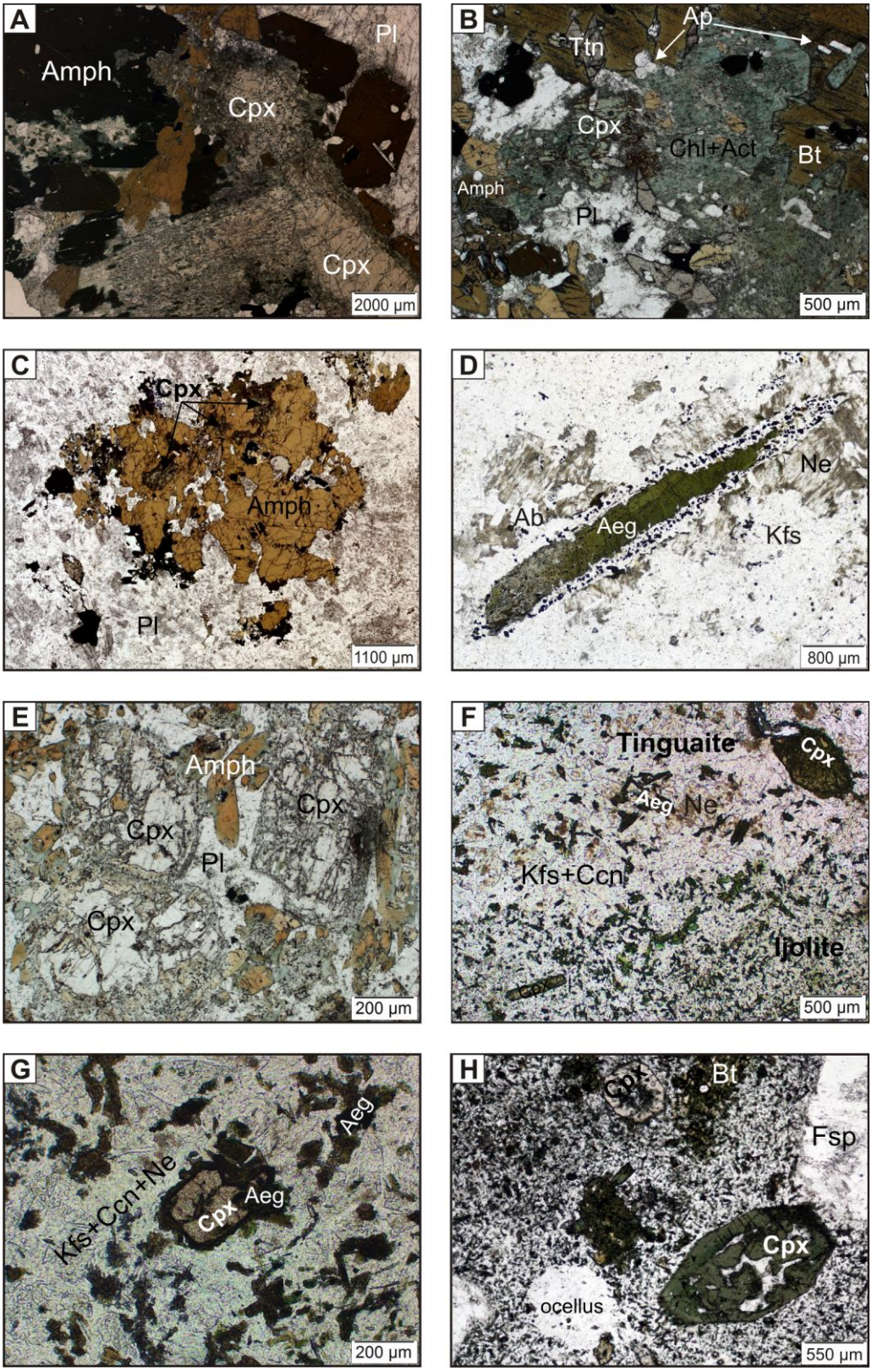


Figure 3

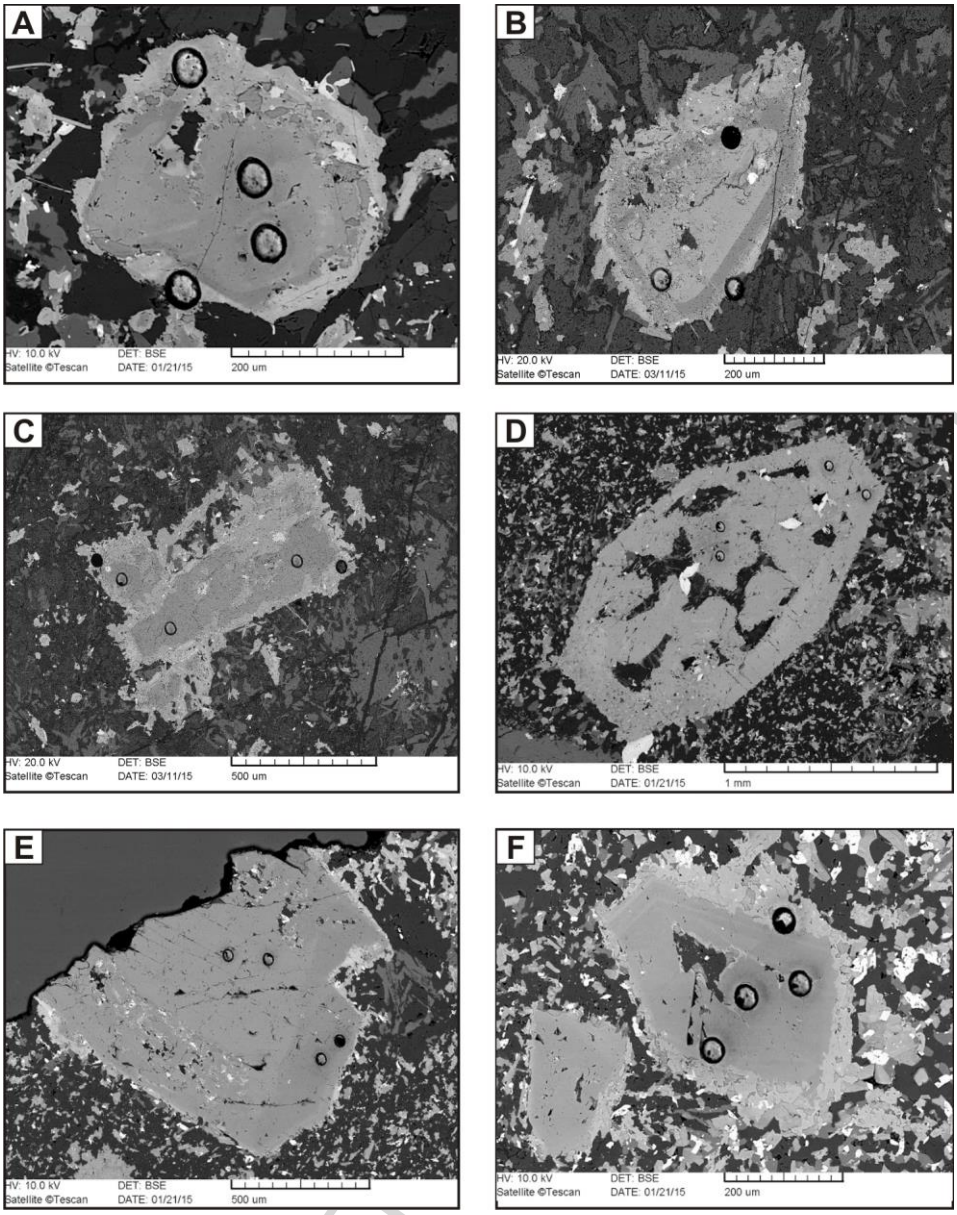


Figure 4

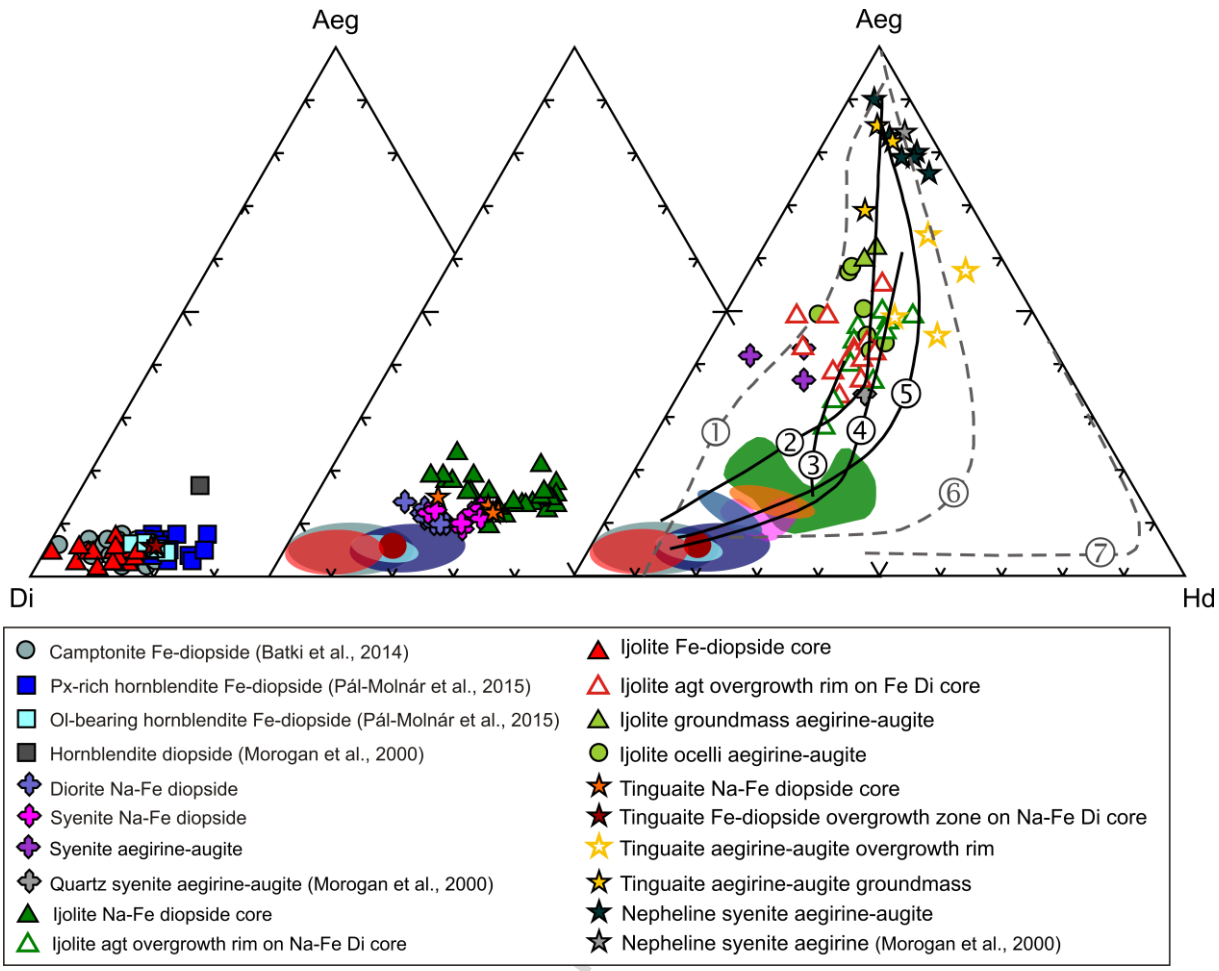


Figure 5

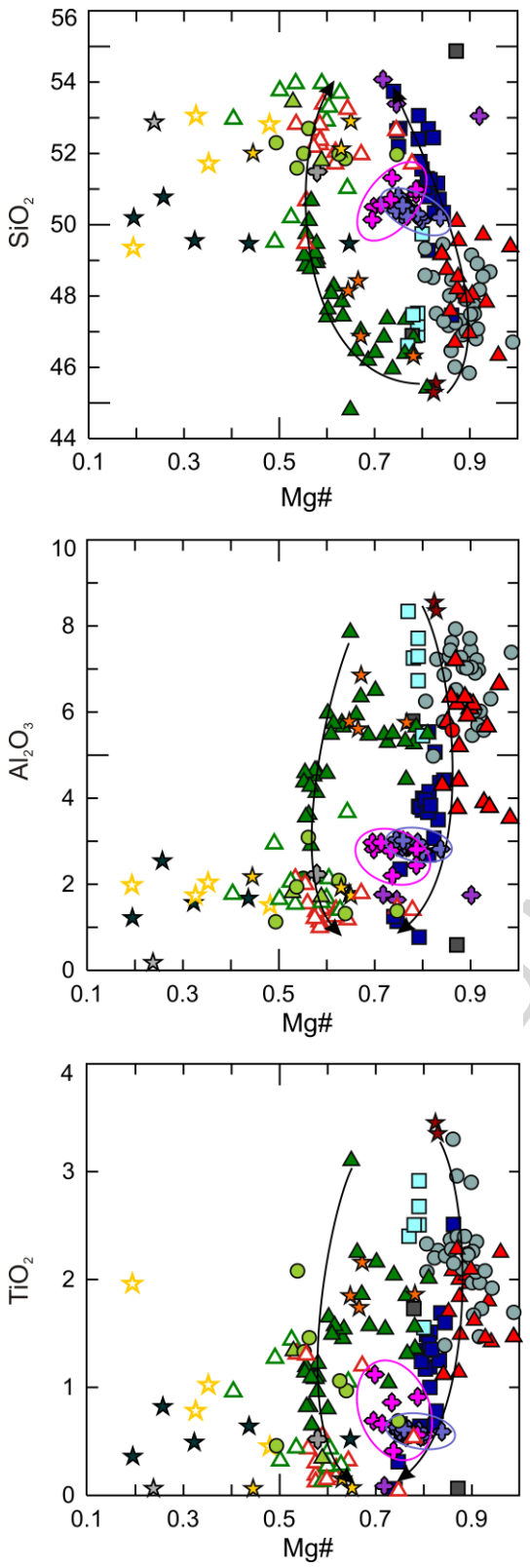


Figure 6

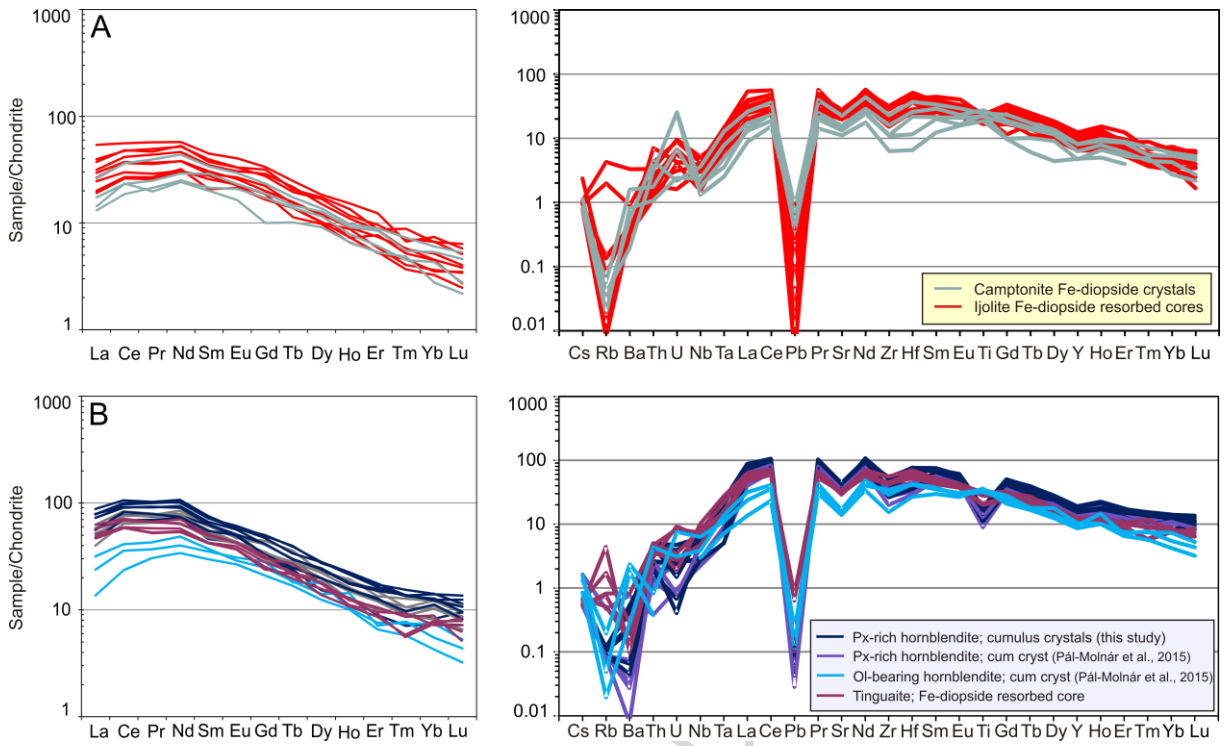


Figure 7

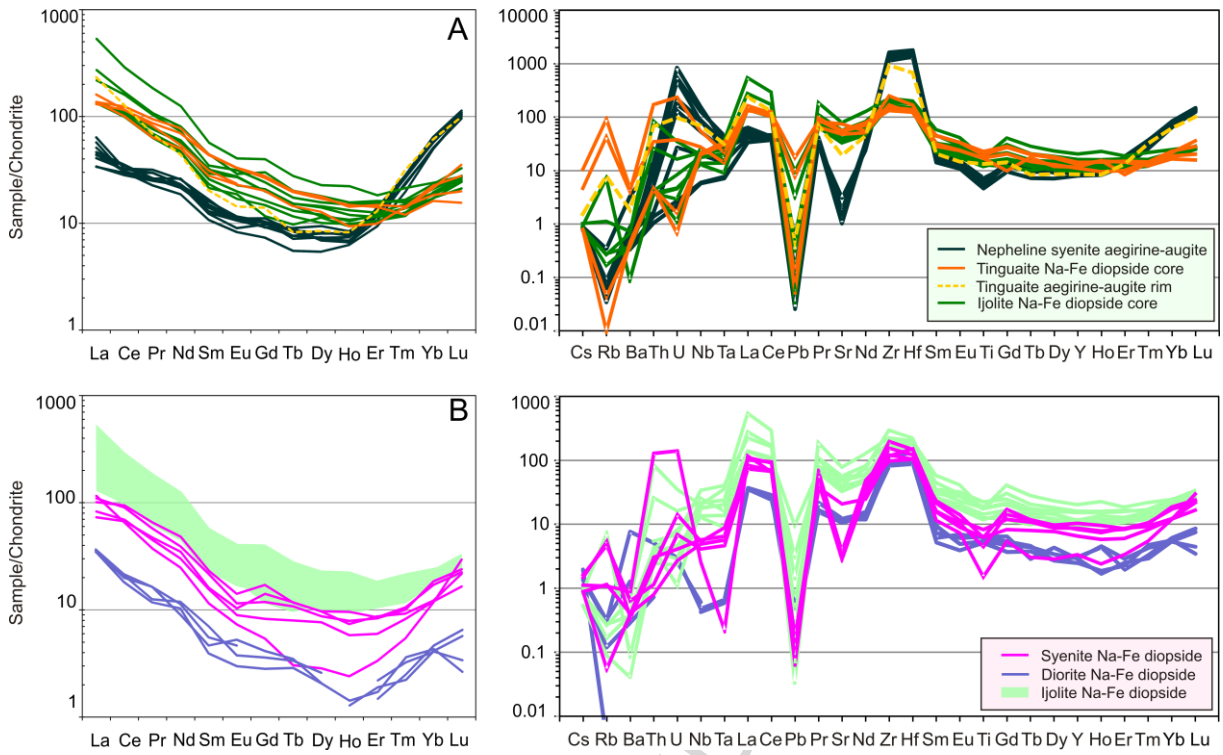


Figure 8

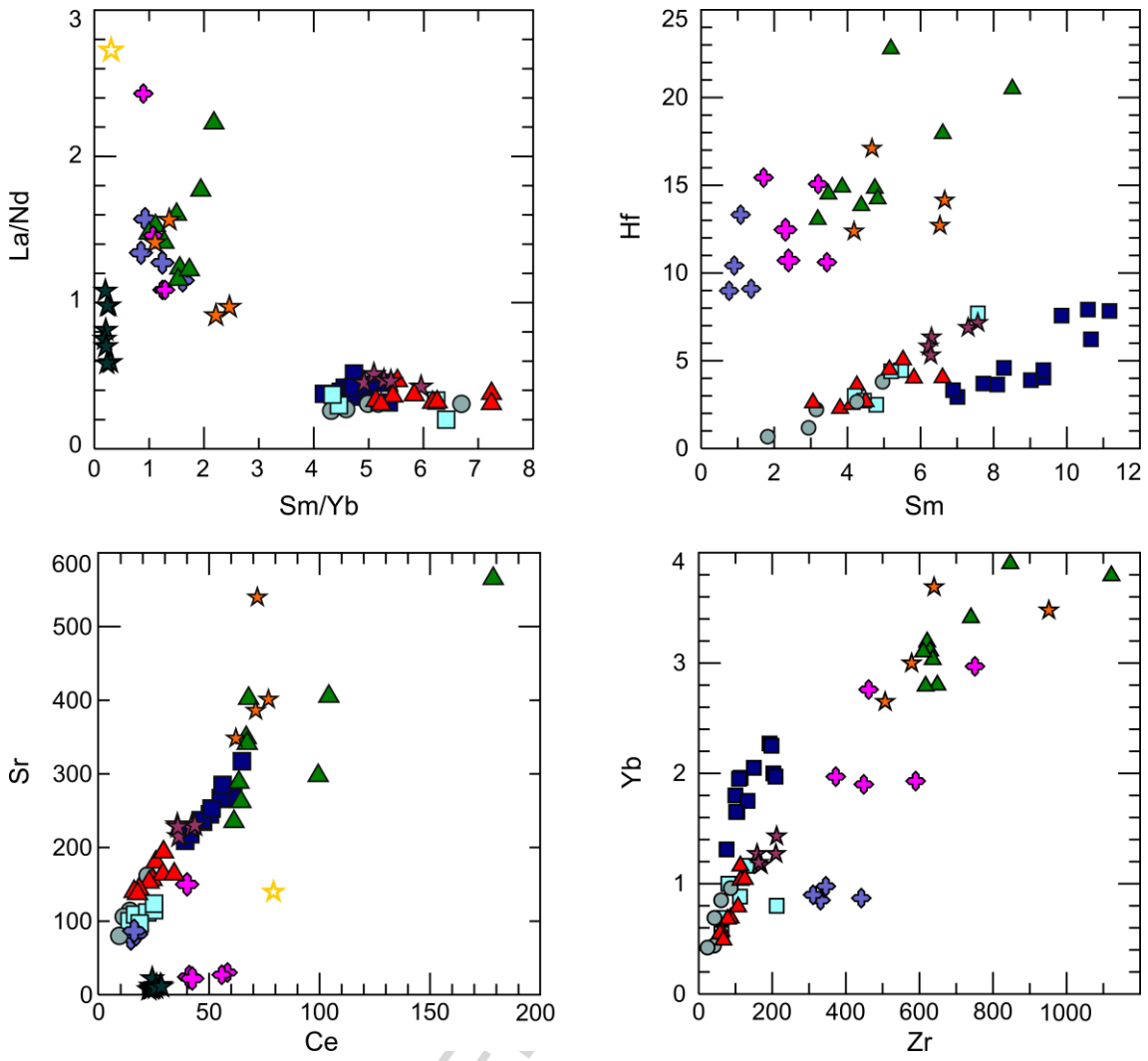


Figure 9

| | Cpx type | Zoning | Texture | Features | Occurrence | Interpretation |
|---|---|---|---|---|---|---|
| **A** | Type I | Unzoned |  | Euhedral-subhedral;<br>77–93 mol% Di, <5540 ppm Cr | Camptonite | phenocryst s.s.<br>crystallisation from M1 |
| **B** | Type I | Unzoned |  | Subhedral, microcryst;<br>72–81 mol% Di, <5360 ppm Cr | Olivine-bearing cumulate | cumulus phase;<br>crystallisation from M1 |
| **C** | Type I | Unzoned |  | Euhedral-subhedral, macrocryst;<br>67–78 mol% Di, <90 ppm Cr | Pyroxene-rich cumulate | cumulus phase,<br>crystallisation from M1a |
| **D** | Type II | Normal |  | Core: euhedral, skeletal, irregular zoning, 10–23 mol% Aeg;<br>rim: subhedral, 28–51 mol% Aeg | Ijolite | core: phenocryst s.s.<br>crystallisation from M2;<br>rim: crystallisation from M2a |
| **E** | Type I<br>(rim: type III) | Normal |  | core: subhedral, sector or oscillatory zoned,<br>80–94 mol% Di, <5290 ppm Cr;<br>rim: subhedral, 35–55 mol% Aeg | Ijolite | core: antecryst,<br>crystallisation from M1;<br>rim: crystallisation from M2a |
| **F** | Type II<br>(mantle: type I,<br>rim: type III) | Multiple |  | Core: anhedral, resorbed,<br>12–15 mol% Aeg;<br>growth zone: 78 mol% Di;<br>rim: 45–64 mol% Aeg | Tinguaite | core: antecryst,<br>crystallisation from M2;<br>growth zone: M1a;<br>rim: crystallised from M2b |
| **G** | Type I<br>(rim: type III) | Normal |  | Core: subhedral, unzoned;<br>10–11 wt.% MgO,<1160 ppm Cr | Tinguaite | core: antecryst,<br>crystallisation from M1a;<br>rim: crystallisation from M2b |
| **H** | Type II | Unzoned |  | Anhedral, partly decomposed,<br>10–13 mol% $Aeg_{syenite}$<br>10–14 mol% $Aeg_{diorite}$ | Syenite<br>Diorite | antecryst,<br>crystallisation from M2 |
| **I** | Type III | Irregular |  | Subhedral, 76–90 mol% Aeg,<br><6260 ppm Zr | Nepheline syenite | phenocryst s.s.<br>crystallisation from M2b |

Figure 10

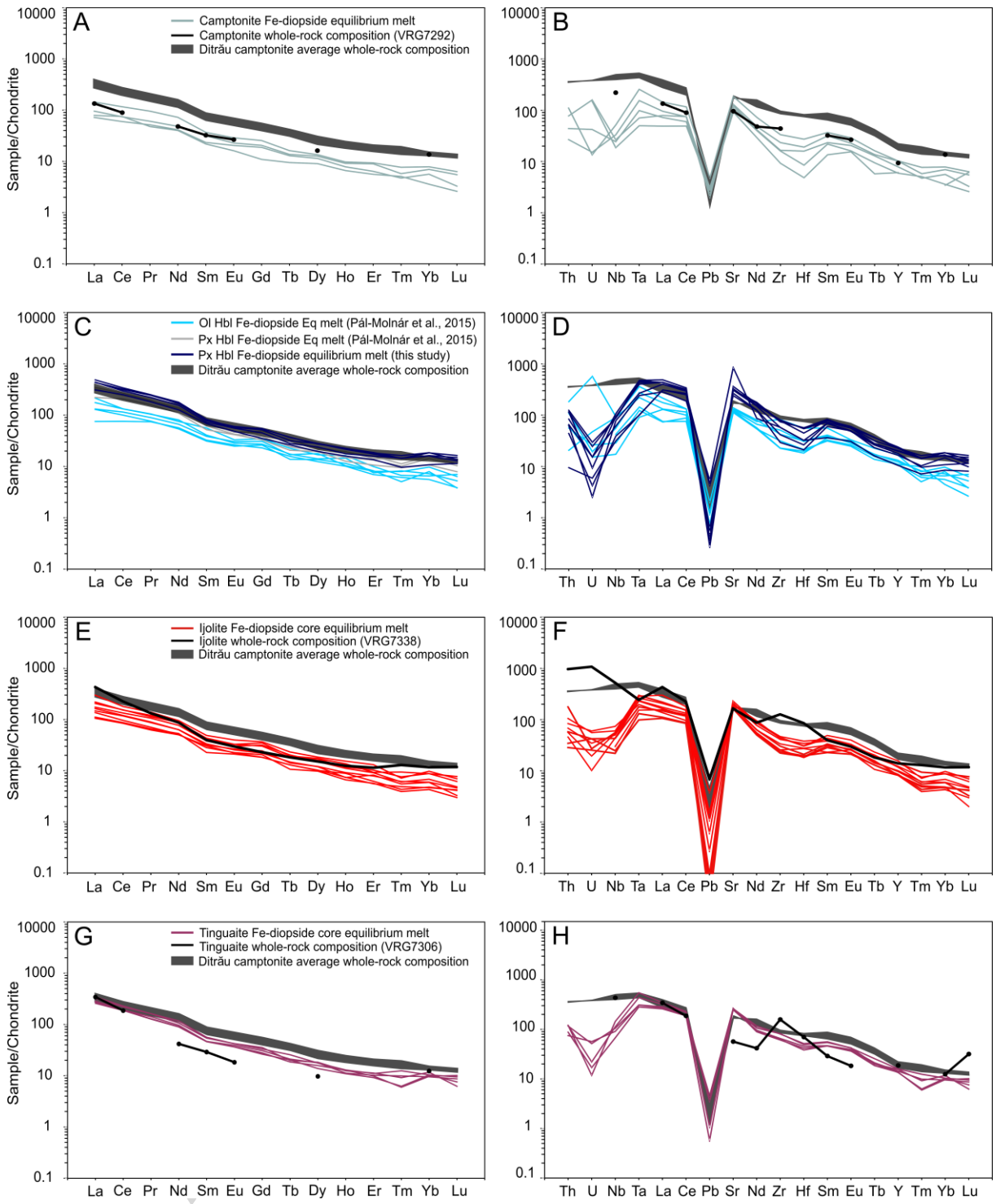


Figure 11

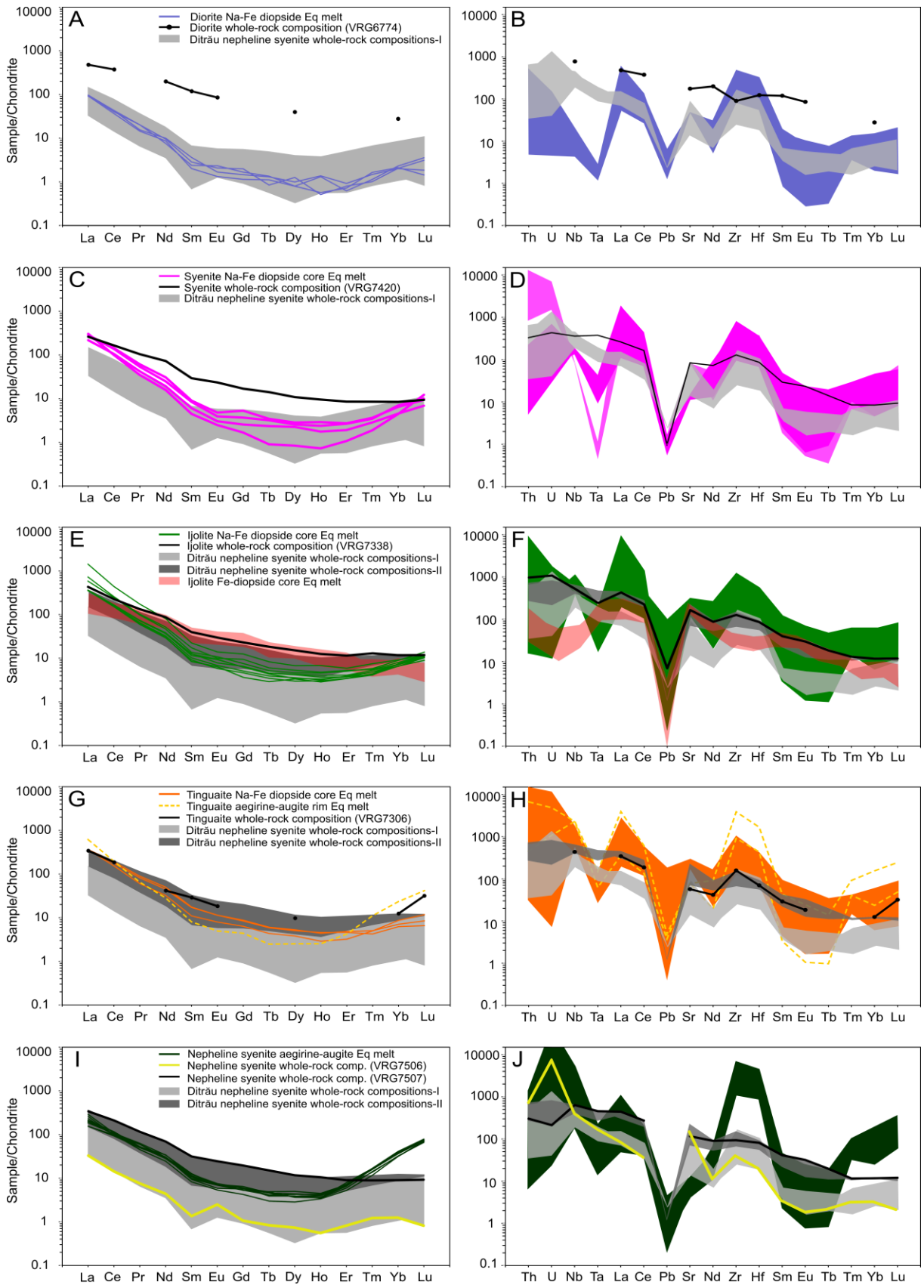


Figure 12

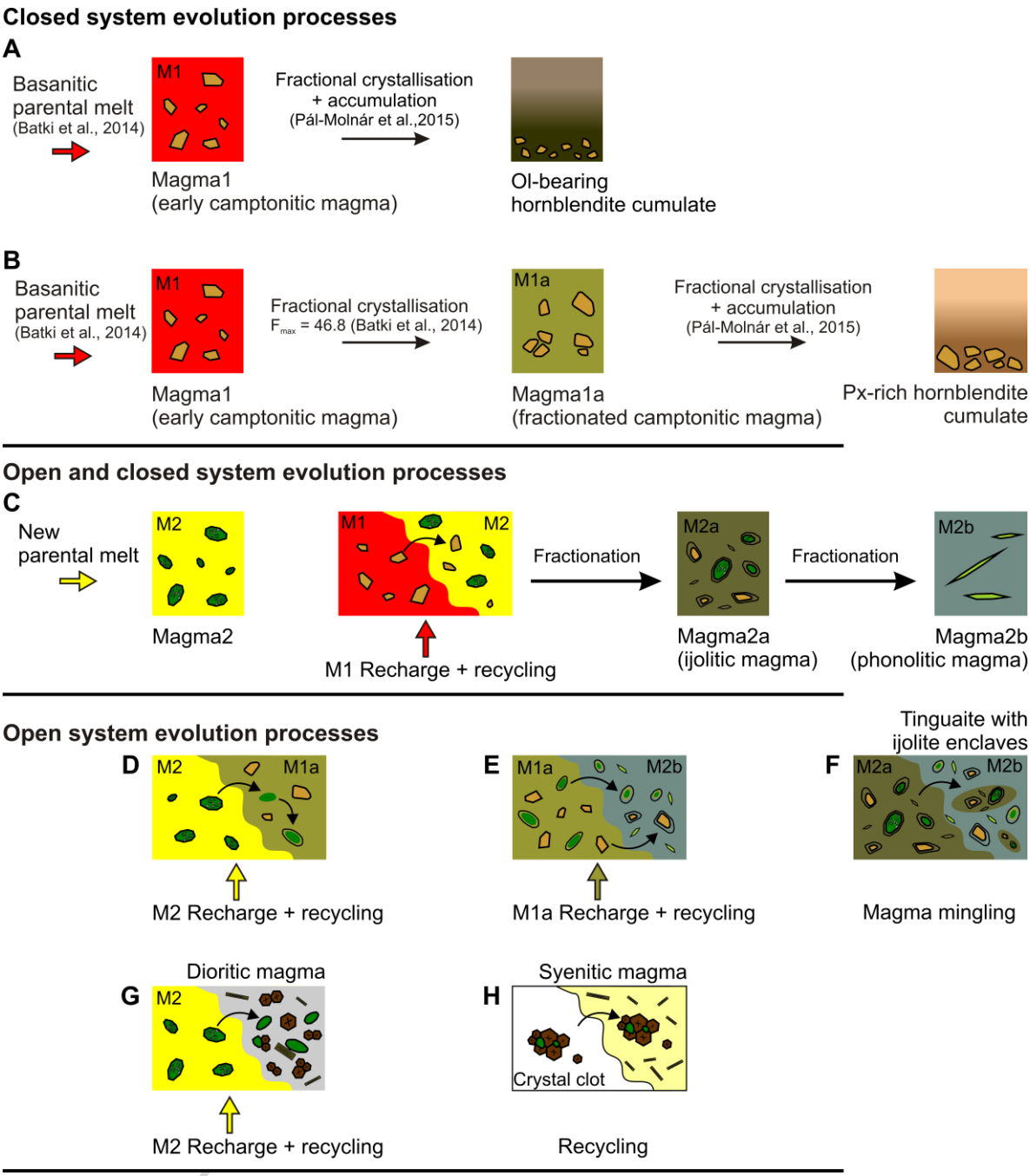


Figure 13

**Table 1.** Mineral assemblage of the investigated samples from the Ditrău Alkaline Massif, Romania

| Phase | Rock type | Phenocrysts* (ph) cumulus minerals (c ) | Groundmass minerals (gr), intercumulus minerals (ic) | Accessory minerals | Secondary minerals | Samples |
|---|---|---|---|---|---|---|
| Cumulate | Ol-bearing Hornblendite | Cpx, ol (c) | Amph (ic) | Ap, mag | Srp, mag | VRG23 |
| Cumulate | Pyroxene-rich Hornblendite | Cpx, amph (c) | Bt, pl (ic) | Ap, ttn, mag | Act, chl, ep | VRG6706 |
| Intrusive | Diorite | Cpx, amph, bt (ph) | – | Ap, ttn, mag | Act, chl, ser | VRG6567 |
| Intrusive | Syenite | Cpx, amph, bt, pl, kfs (ph) | – | Zrn, ap, ttn, mag, rt | Chl, mag, hem, ilm, ep, ms, cal | VRG7420 |
| Intrusive | Nepheline syenite | Aeg, ne, kfs, ab, bt (ph) | – | Zrn, ap, ttn, mag, ilm | Ms, anl, sdl, ccn, mag | VRG6727 |
| Dyke | Camptonite | Cpx (ph) | Amph, bt, pl (gr); ocellus cal | Ap, ttn, mag | Act, chl, mag | VRG7292, VRG7294 |
| Dyke | Tinguaite | Cpx (ph) | Aeg, ne, ab, kfs, ccn (gr) | Zrn, ap, ttn, fl | Bt, ser, mag | VRG7306, VRG7338 |
| Enclave | Ijolite | Cpx (ph) | Aeg, ccn, kfs (gr) | Ap, ttn | Bt, mag | VRG7338, VRG7480 |

*The term "phenocrysts" is used here in a general sense regardless of their origin.

Cpx, clinopyroxene; ol, olivine; amph, amphibole; bt, biotite; pl, plagioclase; kfs, K-feldspar; aeg, aegirine; ne, nepheline; ab, albite; ccn, cancrinite; ap, apatite; mag, magnetite; ttn, titanite; zrn, zircon; rt, rutile; ilm, ilmenite; fl, fluorite; srp, serpentine; act, actinolite; chl, chlorite; ep, epidote; ser, sericite; hem, hematite; ms, muscovite; cal, calcite; anl, analcime; sdl, sodalite.

**Table 2.** Whole-rock major (wt.%) and trace element (ppm) compositions of the studied igneous rocks, Ditrău Alkaline Massif, Romania.

| Location | Pietrăriei de Sus Creek | Pietrăriei de Sus Creek | Teasc Creek | Ditrău Creek | Teasc Creek | Jolotca Creek | Creanga Mare Creek | Creanga Mare Creek | Cetăţii Creeks |
|---|---|---|---|---|---|---|---|---|---|
| Sample | VRG6706 | VRG6774 | VRG7420 | VRG7506 | VRG7507 | VRG7292 | VRG7306 | VRG7338 | VRG7480 |
| Rock type | Px-rich Hornblendite | Diorite | Syenite | Nepheline syenite-I | Nepheline syenite-II | Camptonite dyke | Tinguaite dyke | Ijolite enclave | Ijolite enclave |
| | Pál-Molnár et al. (2015) | | | | | Batki et al. (2014) | | | |
| $SiO_2$ | 32.36 | 43.53 | 60.54 | 57.89 | 55.44 | 45.22 | 57.50 | 49.02 | 45.51 |
| $TiO_2$ | 5.25 | 3.96 | 0.62 | 0.17 | 1.34 | 2.08 | 0.50 | 1.33 | 2.13 |
| $Al_2O_3$ | 9.88 | 14.50 | 19.13 | 21.69 | 18.06 | 12.52 | 21.81 | 18.85 | 16.13 |
| $FeO^t$ | 20.73 | 14.42 | 3.03 | 3.31 | 5.23 | 10.47 | 3.99 | 6.13 | 8.48 |
| MnO | 0.26 | 0.26 | 0.08 | 0.06 | 0.20 | 0.16 | 0.16 | 0.19 | 0.26 |
| MgO | 9.06 | 5.15 | 0.49 | 0.01 | 1.24 | 10.01 | 0.96 | 3.03 | 5.08 |
| CaO | 13.55 | 10.98 | 2.08 | 0.22 | 3.67 | 8.85 | 2.15 | 4.42 | 5.82 |
| $Na_2O$ | 1.77 | 3.54 | 6.12 | 9.32 | 6.48 | 3.01 | 9.38 | 8.17 | 5.75 |
| $K_2O$ | 1.38 | 1.87 | 6.20 | 5.91 | 5.52 | 2.36 | 5.47 | 4.72 | 5.89 |
| $P_2O_5$ | 2.72 | 1.46 | 0.11 | n.d. | 0.22 | 0.26 | 0.08 | 0.35 | 0.42 |
| LOI | 2.60 | n.a. | 1.30 | 1.30 | 2.30 | n.a. | n.a. | 3.20 | 4.10 |
| Total | 99.56 | 99.67 | 99.70 | 99.88 | 99.70 | 94.93 | 102.00 | 99.41 | 99.57 |
| mg# | 0.53 | 0.41 | 0.26 | 0.00 | 0.32 | 0.70 | 0.32 | 0.50 | 0.54 |
| Be | n.d. | 1.86 | n.d. | n.d. | 1 | 1.20 | 4.96 | 12 | 19 |
| Sc | 24 | 10 | 1 | n.d. | 2 | 17 | 1.71 | 6 | 11 |
| V | 356 | 223 | 28 | 43 | 68 | 150 | 29 | 102 | 125 |
| Cr | n.d. | 4.04 | n.d. | n.d. | n.d. | 277 | 20 | 89 | 103 |
| Co | 63 | 32 | 2.1 | 0.8 | 7.8 | 45 | 6.84 | 19 | 25 |
| Ni | 28 | 20 | 0.3 | n.d. | n.d. | 214 | 15 | 46 | 83 |
| Cu | 58 | 81 | 0.7 | n.a. | n.a. | 49 | 16 | 4.1 | 4.4 |
| Zn | 142 | 149 | 52 | n.a. | n.a. | 104 | 124 | 132 | 335 |
| Sr | 778 | 1246 | 610 | 421 | 855 | 695 | 411 | 1200 | 676 |
| Ba | 418 | 616 | 899 | 192 | 767 | 597 | 221 | 1244 | 582 |
| Rb | 29 | 80 | 117 | 114 | 168 | 184 | 467 | 310 | 505 |
| Pb | 2.60 | n.a. | 2.4 | n.a. | n.a. | n.a. | n.a. | 17 | 7.1 |
| Th | 2.70 | n.a. | 9.6 | 8.3 | 8.9 | n.a. | n.a. | 28 | 41.8 |
| U | 1.00 | n.a. | 3.2 | 21.7 | 1.6 | n.a. | n.a. | 8.0 | 8.2 |
| Zr | 160 | 343 | 493 | 60 | 362 | 168 | 602 | 484 | 534 |
| Nb | 48 | 185 | 86 | 37.6 | 155 | 53 | 104 | 126 | 212 |
| Ta | 3.20 | n.a. | 5.1 | 0.9 | 6.3 | n.a. | n.a. | 3.3 | 4.5 |
| Y | 36 | 41 | 14.8 | 1.2 | 22 | 14.7 | 12.9 | 22 | 31 |
| Hf | 4.90 | 12.66 | 8.9 | 0.8 | 8.5 | 8.00 | 7.21 | 8.8 | 7.8 |
| Mo | 1.40 | 3.86 | 2.00 | n.a. | n.a. | 7.80 | 2.13 | 0.4 | 0.4 |
| S | n.a. | 837 | n.a. | n.a. | n.a. | 595 | 135 | n.a. | n.a. |
| La | 71 | 113 | 62 | 7.80 | 106.9 | 32 | 81 | 102 | 133 |
| Ce | 155 | 229 | 101 | 8.70 | 170.5 | 55 | 114 | 138 | 148 |
| Pr | 20 | n.a. | 9.66 | 0.70 | 14.18 | n.a. | n.a. | 12.36 | 13 |
| Nd | 88 | 91 | 33 | 2.00 | 42 | 22 | 19 | 40 | 41 |
| Sm | 17.3 | 17.5 | 4.34 | 0.20 | 6.18 | 4.80 | 4.29 | 5.87 | 6.37 |
| Eu | 5.18 | 4.80 | 1.32 | 0.14 | 1.82 | 1.50 | 1.03 | 1.67 | 2.09 |
| Gd | 15 | n.a. | 3.37 | 0.21 | 5.13 | n.a. | n.a. | 4.58 | 6.22 |
| Tb | 1.94 | n.a. | 0.51 | 0.03 | 0.72 | n.a. | n.a. | 0.66 | 0.89 |
| Dy | 8.89 | 9.76 | 2.66 | 0.18 | 3.80 | 4.00 | 2.39 | 3.72 | 5.01 |
| Ho | 1.36 | n.a. | 0.52 | 0.03 | 0.76 | n.a. | n.a. | 0.68 | 0.92 |
| Er | 3.07 | n.a. | 1.37 | 0.13 | 1.90 | n.a. | 3.20 | 1.83 | 2.68 |
| Tm | 0.38 | n.a. | 0.21 | 0.03 | 0.29 | n.a. | n.a. | 0.32 | 0.38 |
| Yb | 2.21 | 4.46 | 1.36 | 0.20 | 1.91 | 2.20 | 1.99 | 1.88 | 2.46 |
| Lu | 0.31 | n.a. | 0.23 | 0.02 | 0.30 | n.a. | n.a. | 0.29 | 0.27 |

$FeO^t$ as total iron; mg#=Mg/(Mg+$Fe^{2+}$), $Fe^{2+}$ calculated according to Irvine and Baragar (1971); n.a.=not analysed; n.d.=not detected.

**Table 3.** Representative major element compositions (wt.%) of the clinopyroxene populations, Ditrău Alkaline Massif, Romania

| Sample | VRG 6567 | VRG 7420 | VRG 6727 | VRG 7294 | VRG 7338 | VRG 7338 | VRG 7338 | VRG 7338 | VRG 7338 | VRG 7338 | VRG 7338 | VRG 7338 | VRG 7338 | VRG 7338 | VRG 7338 |
|---|---|---|---|---|---|---|---|---|---|---|---|---|---|---|---|
| Rock type | Diorite | Syenite | Nepheline syenite | Camptonite dyke | Tinguaite dyke | Tinguaite dyke | Tinguaite dyke | Tinguaite dyke | Ijolite enclave | Ijolite enclave | Ijolite enclave | Ijolite enclave | Ijolite enclave | Ijolite enclave | Ijolite enclave |
| Spot | Bn518/24 | Bp22 | Bn21 | Tü22 | Up30 | Tü51 | Tü54 | Tü57 | Tü28 | Tü31 | Tü29 | Bp15 | Bp2 | Tü90 | Bp33 |
| Cpx crystal | Antecryst | Antecryst | Phenocr. | Phenocr. | Matrix microlite | Crystal rim (cpx 2) | Antecryst core (cpx 2) | Antecryst growth z. (cpx 2) | Phenocr. core (cpx 1) | Phenocr. core (cpx 1) | Phenocr. rim (cpx 1) | Antecryst rim (cpx 5) | Antecryst core (cpx 6) | Matrix microlite | Ocellus microlite |
| Type | Type II | Type II | Type III | Type I | Type III | Type III | Type II | Type I | Type II | Type II | Type III | Type III | Type I | Type III | Type III |
| Mineral | Na-Fe-diopside | Na-Fe-diopside | Aegirine-augite | Fe-diopside | Aegirine-augite | Aegirine-augite | Na-Fe-diopside | Fe-diopside | Na-Mg Hd | Na-Fe-diopside | Aegirine-augite | Aegirine-augite | Cr-Fe-diopside | Aegirine-augite | Aegirine-augite |
| $SiO_2$ | 50.20 | 50.50 | 50.84 | 48.01 | 52.12 | 53.08 | 48.08 | 45.58 | 49.20 | 47.83 | 52.91 | 52.49 | 48.07 | 53.51 | 51.85 |
| $TiO_2$ | 0.59 | 1.12 | 0.19 | 2.28 | 0.15 | 0.79 | 1.85 | 3.36 | 1.08 | 1.45 | 0.27 | 0.17 | 1.66 | 1.36 | 0.97 |
| $Al_2O_3$ | 2.82 | 2.81 | 1.57 | 7.44 | 1.92 | 1.70 | 5.78 | 8.37 | 4.64 | 5.74 | 1.67 | 1.10 | 6.28 | 1.86 | 1.32 |
| $Cr_2O_3$ | n.a. | n.a. | n.a. | n.a. | 0.02 | n.a. | n.a. | n.a. | n.a. | n.a. | n.a. | 0.00 | 0.68 | n.a. | 0.22 |
| $FeO^t$ | 10.99 | 11.69 | 24.71 | 6.63 | 25.25 | 22.59 | 11.50 | 7.59 | 14.09 | 12.55 | 17.96 | 19.08 | 5.98 | 20.33 | 20.29 |
| MnO | 0.43 | 0.90 | 1.23 | 0.12 | 0.62 | 1.81 | 0.42 | 0.11 | 0.72 | 0.51 | 0.91 | 0.52 | 0.37 | 0.42 | 0.25 |
| MgO | 11.08 | 10.02 | 1.04 | 13.86 | 1.39 | 1.90 | 9.51 | 12.15 | 7.89 | 8.69 | 5.58 | 5.66 | 14.18 | 3.53 | 4.40 |
| $ZrO_2$ | n.a. | n.a. | n.a. | 0.00 | n.a. | 0.67 | 0.05 | 0.02 | 0.08 | 0.13 | 0.25 | n.a. | n.a. | 0.17 | n.a. |
| CaO | 22.12 | 20.97 | 3.35 | 21.60 | 3.49 | 7.53 | 19.59 | 22.01 | 19.39 | 19.94 | 12.07 | 14.84 | 23.11 | 8.06 | 11.82 |
| $Na_2O$ | 1.75 | 1.73 | 11.55 | 0.60 | 11.52 | 9.19 | 1.61 | 0.67 | 2.12 | 1.71 | 6.61 | 5.64 | 0.23 | 9.17 | 7.59 |
| $K_2O$ | 0.02 | 0.00 | 0.00 | 0.03 | 0.00 | 0.02 | 0.00 | 0.00 | 0.00 | 0.02 | 0.01 | n.a. | n.a. | 0.04 | n.a. |
| Total | 100.00 | 99.74 | 94.48 | 100.57 | 96.47 | 99.28 | 98.38 | 99.86 | 99.20 | 98.57 | 98.23 | 99.50 | 100.56 | 98.45 | 98.71 |
| Mg# | 0.84 | 0.70 | 0.99 | 0.86 | 0.63 | 0.33 | 0.65 | 0.83 | 0.58 | 0.63 | 0.60 | 0.59 | 0.91 | 0.53 | 0.64 |
| Di | 70 | 59 | 6 | 82 | 8 | 10 | 56 | 78 | 47 | 53 | 30 | 33 | 88 | 19 | 26 |
| Hd | 15 | 28 | 4 | 14 | 7 | 26 | 32 | 17 | 37 | 33 | 23 | 25 | 10 | 18 | 16 |
| Aeg | 14 | 13 | 90 | 5 | 85 | 64 | 12 | 6 | 16 | 14 | 47 | 42 | 2 | 63 | 58 |

$FeO^t$ as total iron; Phenocr.=Phenocryst; Na-Mg Hd=Na-Mg-hedenbergite; growth z.=growth zone; sector z.=sector zone; n.a.=not analysed.

**Table 4.** Representative trace element compositions (ppm) obtained by LA-ICP-MS on the clinopyroxene populations, Ditrău Alkaline Massif, Romania

| Rock type | Camptonite dyke | Px-rich hornblendite | Ijolite enclave | Ijolite enclave | Ijolite enclave | Tinguaite dyke | Tinguaite dyke | Tinguaite dyke | Nepheline syenite | Nepheline syenite | Syenite | Syenite | Diorite |
|---|---|---|---|---|---|---|---|---|---|---|---|---|---|
| Sample | VRG7292 | VRG6706 | VRG7480 | VRG7338 | VRG7338 | VRG7338 | VRG7338 | VRG7306 | VRG6727 | VRG6727 | VRG7420 | VRG7420 | VRG6567 |
| Crystal type | Phenocryst core | Cumulate macrocryst | Phenocryst core | Phenocryst core | Antecryst core | Antecryst core | Antecryst rim | Antecryst core | Phenocryst core | Phenocryst core | Antecryst core | Antecryst core | Antecryst core |
| Cpx type | Type I | Type I | Type II | Type II | Type I | Type II | Type III | Type I | Type III | Type III | Type II | Type II | Type II |
| Cs | 0.16 | 0.10 | 0.10 | 0.15 | 0.20 | 0.15 | 0.29 | 0.13 | 0.16 | 0.15 | 0.17 | 0.16 | 0.19 |
| Rb | 0.13 | 0.21 | 0.20 | 0.01 | 9.82 | 0.02 | 18.30 | 1.17 | 0.11 | 0.17 | 2.62 | 0.13 | 0.28 |
| Ba | 3.80 | 0.00 | 0.00 | 0.80 | 7.97 | 1.08 | 4.40 | 0.37 | 1.52 | 1.30 | 0.97 | 0.94 | 0.70 |
| Th | 0.05 | 0.05 | 0.16 | 0.12 | 0.10 | 0.14 | 1.94 | 0.14 | 0.05 | 0.28 | 0.02 | 0.09 | 0.02 |
| U | 0.05 | 0.02 | 0.05 | 0.01 | 0.07 | 0.01 | 0.72 | 0.01 | 0.20 | 1.28 | 0.02 | 0.03 | 0.00 |
| Nb | 0.41 | 0.70 | 8.03 | 4.15 | 1.24 | 5.04 | 16.52 | 2.42 | 4.72 | 20.11 | 1.17 | 1.37 | 0.10 |
| Ta | 0.07 | 0.10 | 0.55 | 0.28 | 0.13 | 0.45 | 0.43 | 0.37 | 0.19 | 0.45 | 0.08 | 0.09 | 0.01 |
| La | 3.08 | 13.23 | 52.41 | 31.83 | 5.83 | 32.76 | 55.75 | 14.82 | 9.65 | 13.56 | 23.96 | 26.02 | 8.68 |
| Ce | 11.36 | 50.40 | 98.93 | 66.81 | 18.33 | 76.90 | 79.15 | 43.57 | 25.80 | 23.73 | 57.89 | 55.26 | 17.32 |
| Pb | 1.13 | 0.15 | 3.61 | 0.08 | 0.48 | 0.13 | 1.20 | 0.47 | 0.14 | 0.21 | 0.16 | 0.31 | 1.23 |
| Pr | 1.97 | 7.33 | 9.71 | 7.33 | 2.69 | 8.88 | 6.47 | 6.17 | 3.64 | 3.62 | 6.07 | 5.31 | 2.00 |
| Sr | 106 | 245 | 297 | 349 | 151 | 401 | 141 | 230 | 9 | 12 | 27 | 24 | 88 |
| Nd | 11.36 | 33.90 | 33.48 | 27.51 | 14.09 | 35.86 | 20.40 | 29.09 | 13.81 | 13.87 | 22.04 | 17.83 | 6.81 |
| Zr | 43 | 100 | 1122 | 610 | 67 | 579 | 3550 | 212 | 6257 | 5344 | 462 | 751 | 442 |
| Hf | 2.22 | 3.64 | 22.85 | 14.82 | 2.53 | 14.15 | 69.08 | 6.88 | 184.00 | 176.20 | 10.61 | 15.07 | 13.32 |
| Sm | 3.15 | 8.10 | 5.19 | 4.75 | 3.80 | 6.66 | 3.05 | 7.30 | 2.53 | 2.84 | 3.44 | 3.20 | 1.08 |
| Eu | 1.17 | 2.81 | 1.78 | 1.56 | 1.29 | 1.89 | 0.82 | 2.41 | 0.81 | 0.85 | 0.79 | 0.65 | 0.34 |
| Gd | 3.40 | 6.55 | 4.85 | 4.00 | 3.72 | 5.60 | 2.82 | 6.43 | 2.65 | 2.36 | 3.40 | 2.36 | 1.27 |
| Tb | 0.49 | 0.89 | 0.63 | 0.55 | 0.41 | 0.74 | 0.30 | 0.76 | 0.40 | 0.43 | 0.42 | 0.39 | 0.10 |
| Dy | 2.81 | 4.84 | 3.89 | 3.59 | 2.41 | 4.44 | 2.12 | 4.49 | 2.29 | 3.03 | 2.39 | 2.15 | 1.06 |
| Y | 9.7 | 20.6 | 23.8 | 18.0 | 10.1 | 22.4 | 13.4 | 19.2 | 15.7 | 15.2 | 16.3 | 13.6 | 4.5 |
| Ho | 0.42 | 0.85 | 0.82 | 0.73 | 0.36 | 0.79 | 0.46 | 0.67 | 0.49 | 0.60 | 0.52 | 0.43 | 0.09 |
| Er | 0.96 | 2.00 | 2.50 | 2.03 | 0.86 | 2.41 | 2.11 | 1.70 | 2.45 | 2.65 | 1.36 | 1.33 | 0.40 |
| Tm | 0.11 | 0.24 | 0.41 | 0.38 | 0.09 | 0.36 | 0.79 | 0.21 | 0.89 | 0.86 | 0.26 | 0.25 | 0.07 |
| Yb | 0.69 | 1.80 | 3.79 | 3.10 | 0.53 | 3.00 | 9.95 | 1.43 | 12.16 | 12.01 | 2.76 | 2.97 | 0.87 |
| Lu | 0.07 | 0.20 | 0.81 | 0.64 | 0.06 | 0.50 | 2.46 | 0.13 | 3.51 | 3.50 | 0.55 | 0.59 | 0.18 |
| V | 219 | 123 | 354 | 296 | 139 | 285 | 184 | 210 | 125 | 188 | 129 | 125 | 231 |
| Cr | 3158 | 36 | 10 | 14 | 5288 | 34 | 11 | 1159 | 8 | 9 | 10 | 12 | 1.2 |
| Ni | 202 | 77 | 6 | 25 | 209 | 28 | 12 | 108 | 5 | 5 | 6 | 6 | 6 |

Graphical Abstract (for review)

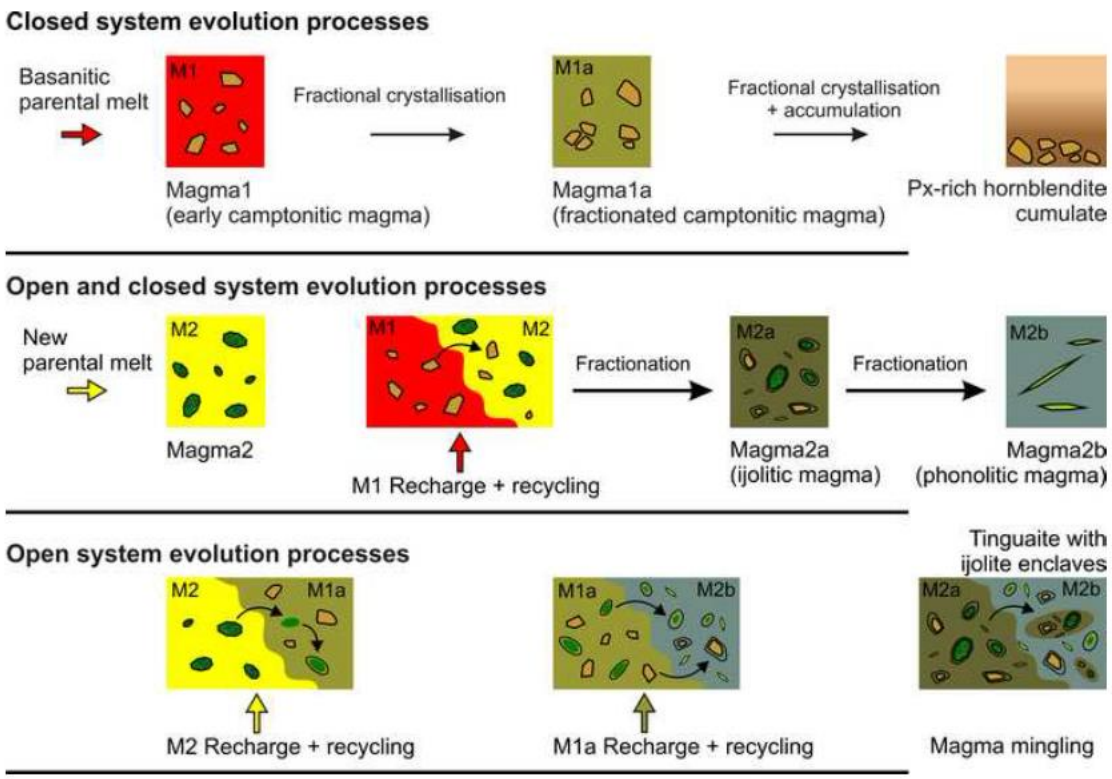


Graphical abstract

Highlights

1. Clinopyroxenes record two magma sources and evolution trends in the Ditrău plutonic system
2. A new, Nb and Zr rich parental melt has been recognised in the Ditrău magmatic system
3. Zoning patterns and trace element variations reveal open- and closed system processes
4. Magma recharge triggers mingling and antecryst recycling between mafic and felsic magmas
5. Incorporated clinopyroxene antecrysts crucially affect the host magma composition